

The 6dF Galaxy Survey: Bulk Flows on $50 - 70 h^{-1}$ Mpc scales

Morag I. Scrimgeour^{1,2,3,4*}, Tamara M. Davis⁵, Chris Blake⁶, Lister Staveley-Smith^{3,4}, Christina Magoulas^{7,8,9}, Christopher M. Springob^{3,4,9}, Florian Beutler¹⁰, Matthew Colless¹¹, Andrew Johnson⁶, D. Heath Jones^{12,13}, Jun Koda^{4,6}, John R. Lucey¹⁴, Yin-Zhe Ma¹⁵, Jeremy Mould^{4,6} and Gregory B. Poole⁸

¹ Department of Physics and Astronomy, University of Waterloo, Waterloo, ON, N2L 3G1, Canada

² Perimeter Institute for Theoretical Physics, 31 Caroline St. N., Waterloo, ON, N2L 2Y5, Canada

³ International Centre for Radio Astronomy Research, M468, University of Western Australia, 35 Stirling Hwy, Crawley, WA 6009, Australia

⁴ ARC Centre of Excellence for All-sky Astrophysics (CAASTRO)

⁵ School of Mathematics and Physics, University of Queensland, Brisbane, QLD 4072, Australia

⁶ Centre for Astrophysics & Supercomputing, Swinburne University of Technology, P.O. Box 218, Hawthorn, VIC 3122, Australia

⁷ Department of Astronomy, University of Cape Town, Private Bag X3, Rondebosch, 7701, South Africa

⁸ School of Physics, University of Melbourne, Parkville, VIC, 3010, Australia

⁹ Australian Astronomical Observatory, PO Box 915, North Ryde, NSW, 1670, Australia

¹⁰ Lawrence Berkeley National Lab, 1 Cyclotron Rd, Berkeley CA 94720, USA

¹¹ Research School of Astronomy & Astrophysics, Australian National University, Australia

¹² Department of Physics and Astronomy, Macquarie University, Sydney, NSW 2109, Australia

¹³ School of Physics, Monash University, Clayton, VIC 3800, Australia

¹⁴ Department of Physics, University of Durham, Durham DH1 3LE, UK

¹⁵ Astrophysics and Cosmology Research Unit, School of Chemistry and Physics, University of KwaZulu-Natal, Durban, South Africa

ABSTRACT

We measure the bulk flow of the local Universe using the 6dF Galaxy Survey peculiar velocity sample (6dFGSv), the largest and most homogeneous peculiar velocity sample to date. 6dFGSv is a Fundamental Plane sample of $\sim 10^4$ peculiar velocities covering the whole southern hemisphere for galactic latitude $|b| > 10^\circ$, out to redshift $z = 0.0537$. We apply the ‘Minimum Variance’ bulk flow weighting method, which allows us to make a robust measurement of the bulk flow on scales of 50 and $70 h^{-1}$ Mpc. We investigate and correct for potential bias due to the lognormal velocity uncertainties, and verify our method by constructing Λ CDM 6dFGSv mock catalogues incorporating the survey selection function. For a hemisphere of radius $50 h^{-1}$ Mpc we find a bulk flow amplitude of $U = 248 \pm 58 \text{ km s}^{-1}$ in the direction $(l, b) = (318^\circ \pm 20^\circ, 40^\circ \pm 13^\circ)$, and for $70 h^{-1}$ Mpc we find $U = 243 \pm 58 \text{ km s}^{-1}$, in the same direction. Our measurement gives us a constraint on σ_8 of $1.01^{+1.07}_{-0.58}$. Our results are in agreement with other recent measurements of the direction of the bulk flow, and our measured amplitude is consistent with a Λ CDM prediction.

Key words: surveys – galaxies: statistics – cosmology: observations – large-scale structure of Universe – galaxies: kinematics and dynamics

1 INTRODUCTION

The standard model of cosmology, Lambda Cold Dark Matter (Λ CDM) is now well supported by a wide variety of observational probes, yet questions still remain about the nature of dark matter, and whether the observed cosmic expan-

sion is caused by a cosmological constant, Λ , or some other form of dark energy. Galaxy peculiar velocities are one of the only probes of large-scale structure in the nearby Universe, and are gaining interest as a promising cosmological probe that offers new information on these problems at low redshift. Peculiar velocities are the motions of galaxies caused by gravitational infall into local matter overdensities. They are usually measured statistically via redshift-space distor-

* E-mail: morag.astro@gmail.com

tions (Kaiser 1987; Peacock et al. 2001; Tegmark et al. 2004; Guzzo et al. 2008) but can also be measured directly. The line-of-sight component of the peculiar velocity \mathbf{v} of a galaxy at position \mathbf{r} is given by

$$v \equiv \mathbf{v} \cdot \hat{\mathbf{r}} = c \left(\frac{z_{\text{obs}} - z_r}{1 + z_r} \right), \quad (1)$$

where c is the speed of light, z_{obs} is the observed redshift, measured spectroscopically and corrected to the CMB rest-frame, and z_r is the redshift corresponding to the real-space comoving distance r of the galaxy.¹ The hat on $\hat{\mathbf{r}}$ denotes the unit vector.

In the linear regime, the velocity field $\mathbf{v}(\mathbf{r})$ is directly related to the density field $\delta(\mathbf{r})$, via (Peebles 1980)

$$\mathbf{v}(\mathbf{r}) = \frac{H_0 a f}{4\pi} \int d^3 \mathbf{r}' \frac{\delta(\mathbf{r}')(\mathbf{r}' - \mathbf{r})}{|\mathbf{r}' - \mathbf{r}|^3}, \quad (2)$$

where $f \equiv d \ln D / d \ln a$ is the present-day growth rate of cosmic structure (in terms of the linear growth factor D and cosmic scale factor a), and $\delta(\mathbf{r}) = [\rho(\mathbf{r}) - \bar{\rho}] / \bar{\rho}$ with $\bar{\rho}$ the average density of the Universe. Peculiar velocity measurements therefore allow us to trace the total matter distribution, including dark matter, without the complication of galaxy bias, and over a large range of scales. They also probe the nature of gravity through the growth rate f .

The dipole of the velocity field, or ‘bulk flow’ is particularly interesting since it measures the large-scale streaming motion of matter in the local Universe, which is sensitive to the large-scale modes of the matter power spectrum, and the matter density. There has been a lot of interest in the bulk flow on scales of $50 - 100 h^{-1}$ Mpc, since some authors have suggested it is larger than expected in Λ CDM; however, there has been a history of conflicting results in the literature. Some early measurements gave indications of apparently large bulk flows (Rubin et al. 1976; Dressler et al. 1987a; Lynden-Bell et al. 1988), while others found values consistent with predictions (Hart & Davies 1982; de Vaucouleurs & Peters 1984; Aaronson et al. 1986) – see Kaiser (1988) and Strauss & Willick (1995) for a review of early measurements. More recently, an increase in the amount and quality of peculiar velocity data has led to a surge of new measurements. Again, some of these claimed to find evidence of an unusually large bulk flow (Kashlinsky et al. 2008; Watkins et al. 2009; Feldman et al. 2010; Abate & Feldman 2012), while most find results consistent with Λ CDM (Colin et al. 2011; Nusser & Davis 2011; Osborne et al. 2011; Dai et al. 2011; Turnbull et al. 2012; Lavaux et al. 2013; Ma & Scott 2013; Planck Collaboration et al. 2014b; Carrick et al. 2014; Ma & Pan 2014; Hong et al. 2014; Feix et al. 2014).

Some reported detections of unusually large bulk flows have been directly challenged. Kashlinsky et al. (2008) claimed to find a large dipole in the WMAP kinetic Sunyaev-Zel’dovich (kSZ) effect, indicating a bulk flow of 600-1000 km s^{-1} out to $z \sim 0.1$, while Keisler (2009) showed their uncertainties were underestimated, reducing the significance of

their result. Watkins et al. (2009) combined several different peculiar velocity catalogues, and used a ‘minimum variance’ bulk flow estimator to find a bulk flow of 407 km s^{-1} on a scale of $50 h^{-1}$ Mpc, while Ma & Scott (2013) repeated their analysis using a hyperparameter method to combine the surveys, along with a different choice of velocity dispersion parameter, and found a smaller bulk flow consistent with Λ CDM. Large-scale bulk flows also appear to contradict measurements of large-scale homogeneity in the galaxy distribution by Hogg et al. (2005) and Scrimgeour et al. (2012). Hence, although a large bulk flow remains an intriguing possibility, it could be attributed to unaccounted-for systematic or statistical errors in existing measurements.

Another aim of measuring the large scale bulk flow is to put in context the motion of the Local Group (LG) with respect to the CMB, i.e. the bulk flow on the scale of a few Mpc. The LG motion is $627 \pm 22 \text{ km s}^{-1}$ towards $l = 276 \pm 3^\circ, b = 30 \pm 2^\circ$ (Kogut et al. 1993). In the gravitational instability model of linear theory, this is expected to be influenced by both nearby and large scale structures, and would converge to the CMB dipole when averaging over a region of sufficiently large radius. However, attempts to reconstruct the CMB dipole using the density field have been inconsistent. Studies have suggested that it is necessary to go to scales of at least that of the Shapley Supercluster at $150 h^{-1}$ Mpc to recover the dipole motion (Kocevski & Ebeling 2006; Muñoz & Loeb 2008; Lavaux et al. 2010) while Erdoğan et al. (2006a,b) suggest only $\sim 30\%$ of the motion is due to structures beyond $50 h^{-1}$ Mpc. Other studies show no convergence up to $200 - 300 h^{-1}$ Mpc (Bilicki et al. 2011; Nusser et al. 2014).

In this work we aim to shine new light on the local bulk flow, using peculiar velocity data from the 6-degree Field Galaxy Survey (6dFGS, Jones et al. 2004; Magoulas et al. 2012). This dataset is the largest, most homogeneously derived peculiar velocity sample to date, with 8885 Fundamental Plane distances. We apply the optimal Minimum Variance weighting method proposed by Watkins et al. (2009); Feldman et al. (2010) to measure the bulk flow.

This paper is structured as follows. In Section 2 we describe the 6dFGSv peculiar velocity sample. In Section 3 we explain how we derive peculiar velocities from the logarithmic distances, and our method of defining the velocity uncertainty of each galaxy to avoid bias in the estimated bulk flow. In Section 4 we describe the Maximum Likelihood and Minimum Variance methods that we use to estimate the bulk flow. In Section 5 we describe our Λ CDM-based 6dFGSv mock catalogues. We present and discuss our results in Section 6 and conclude in Section 7.

Throughout this work we assume a flat Λ CDM cosmology with parameters from the *Planck* 2013 data release, of $\Omega_m = 0.3175$, $\Omega_\Lambda = 0.6825$, $\sigma_8 = 0.8344$, and $H_0 = 100h \text{ km s}^{-1} \text{ Mpc}^{-1}$ with $h = 0.67$. We only use this cosmology when converting between distance and redshift, and for comparing our bulk flow results with the Λ CDM predicted velocity dispersion. Since 6dFGSv is at low redshift ($z \leq 0.054$) the results are only weakly dependent on the values of the cosmological parameters we assume. The uncertainties on these parameters are also significantly smaller than the uncertainties on our measurement, assuming a Λ CDM model, and so we fix these parameters throughout this work, since varying them would have a negligible effect.

¹ Equation 1 is often approximated in the literature as $v = cz_{\text{obs}} - H_0 D$, where H_0 is the Hubble constant and D is the proper distance to the galaxy. However, this is only accurate for $z \ll 0.1$ (Harrison 1993; Davis & Lineweaver 2004; Davis & Scrimgeour 2014).

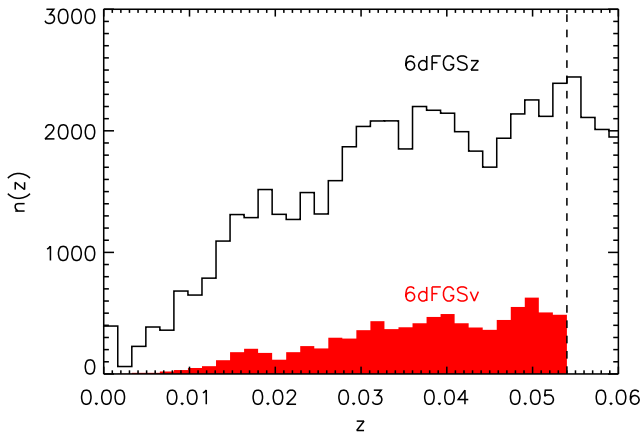


Figure 1. Redshift distribution of the 6dFGS peculiar velocity sample (6dFGSv, solid red histogram) compared to the parent J-band spectroscopic sample (6dFGSz, black line histogram). The vertical dashed line shows the redshift cut imposed on the velocity sample.

2 6dFGS PECULIAR VELOCITY SAMPLE

The 6-degree field Galaxy Survey (6dFGS) is a combined redshift and peculiar velocity survey of almost the whole southern hemisphere, performed using the Six-Degree Field (6dF) multi-fibre spectrograph on the UK Schmidt Telescope from May 2001 to January 2006 (Jones et al. 2004, 2006, 2009). The survey covers galactic latitudes $|b| > 10^\circ$ out to a redshift of $z \sim 0.15$. The redshift survey (6dFGSz) contains 125 071 near-infrared (NIR) and optically selected spectroscopic galaxy redshifts, over $17\,000\text{ deg}^2$ and with a median redshift of 0.053. Targets were selected in the *JHK* bands from the 2MASS Extended Source Catalog (2MASS XSC; Jarrett et al. 2000), with secondary samples in the b_J and r_F bands.

The peculiar velocity sample, denoted 6dFGSv (Campbell 2009; Campbell et al. 2014), is a subset of 8885 bright, early-type galaxies for which distances were derived using the Fundamental Plane (FP) relation. This sample was drawn from $\sim 11\,000$ galaxies in 6dFGSz with measured FP data, in the form of velocity dispersions and photometric scalelengths (Campbell et al. 2014). The sample was selected by requiring good redshift quality ($Q = 3 - 5$), *J*-band magnitude $J < 13.75$, redshifts less than $16\,500\text{ km s}^{-1}$ (or $z < 0.0537$), and velocity dispersions larger than $\sigma_0 \geq 112\text{ km s}^{-1}$, with signal-to-noise $S/N > 5\text{ \AA}^{-1}$.

The redshift distribution of 6dFGSv compared to that of the parent J-band 6dFGSz sample is shown in Figure 1. The fitting of the FP, and the selection cuts applied to obtain the FP and peculiar velocity samples, are described in detail in Magoulas et al. (2012) (hereafter M12). The derivation of the FP distances and peculiar velocities, and correction for Malmquist bias and other selection effects, is described in Springob et al. (2014) (hereafter S14).

3 DERIVING PECULIAR VELOCITIES FOR 6dFGSv

The output of the FP peculiar velocity derivation for 6dFGSv (from S14) is a probability distribution for the ‘logarithmic distance ratio’ for each galaxy, η , defined by

$$\eta \equiv \log_{10}(D_z/D_r), \quad (3)$$

where D_z is the co-moving distance in the fiducial Λ CDM cosmology corresponding to the observed redshift z , while D_r is the co-moving distance corresponding to the angular diameter distance inferred from the Fundamental Plane.

Instead of obtaining η as a single value with an uncertainty, S14 derive the full posterior probability distributions $P(\eta)$, in order to retain all the available information resulting from the selection cuts on the FP. These probability distributions are close to Gaussian in log distance, with a small skew due to the different selection effects and bias corrections, as described in S14.

The optimal ‘Minimum Variance’ estimator we wish to use for the bulk flow measurement, described in the next section, takes as input peculiar velocities in km s^{-1} . To convert η to peculiar velocity v , we use the fact that

$$(1+z) = (1+z_r)(1+z_p) \quad (4)$$

where z_r is the redshift corresponding to D_r in the assumed cosmology, and z_p is the ‘peculiar redshift,’ $z_p = v/c$, where v is the line-of-sight component of the galaxy’s peculiar velocity. The relation between redshift and co-moving distance is

$$D(z) = \frac{c}{H_0} \int_0^z \frac{dz'}{E(z')} \quad (5)$$

where

$$E(z) = \frac{H(z)}{H_0} = [\Omega_m(1+z)^3 + \Omega_\Lambda]^{1/2}, \quad (6)$$

for which we use the fiducial Λ CDM parameter values listed in Section 1.

The peculiar velocity v corresponding to η is then

$$v(\eta, z) = c \left(\frac{z - z_r(\eta, z)}{1 + z_r(\eta, z)} \right), \quad (7)$$

with z_r obtained from η and z using Eqs. 3 and 5. This relation for $v(\eta, z)$ is illustrated for the 6dFGSv sample in Figure 2.

We see that $v(\eta, z)$ is nonlinear at fixed redshift, which poses a problem for obtaining an unbiased estimate of v . The observable quantity η has Gaussian uncertainty in log-space, which translates to lognormal uncertainty on v . This is a standard problem for peculiar velocity measurements.

We can see this by converting the $P(\eta)$ distributions to probability distributions of velocity, $P(v)$, using the relation

$$P(v) = P(\eta) \frac{d\eta}{dv} = P(\eta) \frac{1}{D_r \ln(10)} \frac{dD_r}{dz_r} \frac{(1+z_r)^2}{c(1+z)}, \quad (8)$$

where \ln is the natural logarithm. A typical velocity probability distribution $P(v)$ is illustrated in Figure 3, where we have set $\langle \eta \rangle \equiv 0$. The distribution is close to lognormal.

We obtain the peculiar velocity for each galaxy by taking the mean value of the $P(\eta)$ distribution, $\langle \eta \rangle = \int_{-\infty}^{\infty} \eta P(\eta) d\eta$, and converting it to velocity using Eq. 7. This is equivalent to the median of the $P(v)$ distribution, as can

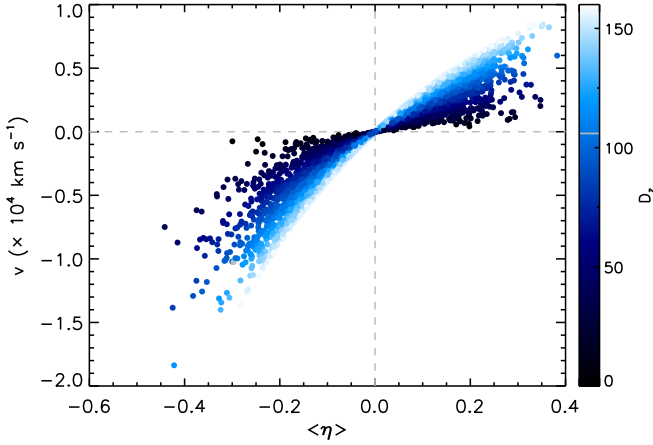


Figure 2. Radial peculiar velocity v from Equation 7, as a function of the mean η value of each galaxy, $\langle\eta\rangle$, for the 6dFGSv sample, colour-coded by redshift distance D_z . The $v(\eta)$ relation is single-valued and monotonic for a given D_z , and is increasingly nonlinear for increasing D_z .

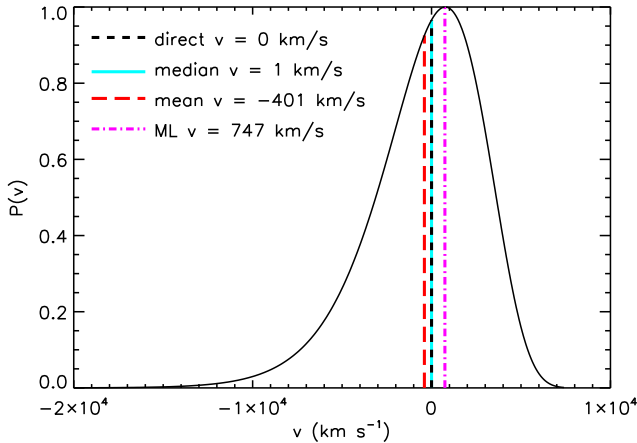


Figure 3. A typical $P(v)$ distribution for 6dFGSv, for an imagined galaxy at the mean redshift of 6dFGSv, and having the mean η uncertainty, σ_η , of the sample, but with $\langle\eta\rangle \equiv 0$. The red long-dashed line is the mean of $P(v)$, the magenta dot-dashed line is the maximum likelihood, the cyan solid line is the median and the black short-dashed line is the direct conversion of $\langle\eta\rangle$ to v , which is almost identical to the median. Since $\langle\eta\rangle$ is zero, the peculiar velocity of the galaxy should be zero, but only the median and the direct $\langle\eta\rangle \rightarrow v$ have this value.

be seen in Fig. 3. This is the least biased way to determine velocity, correctly giving zero v for zero η , and it is also the standard method used in the literature.

Since the uncertainty on η is Gaussian, the uncertainty on v is lognormal, and is proportional to D_z . The uncertainty on v , as derived from $P(v)$, is also proportional to v , since the width of $P(v)$ increases with radial velocity. To derive the velocity uncertainties as approximate Gaussian uncertainties, σ_v , which we need for the Minimum Variance estimator, we first calculate the standard deviation of each

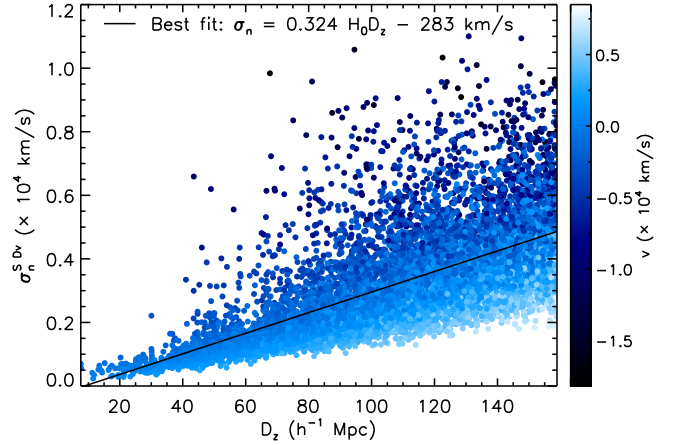


Figure 4. The correlation between the standard deviation $\sigma_n^{\text{SD}v}$ of $P(v)$, and redshift distance D_z . The colour gradient shows the corresponding peculiar velocity. A linear best-fit to the points is shown in black.

$P(v)$ distribution,

$$\sigma_n^{\text{SD}v} = \left(\int_{-\infty}^{\infty} v^2 P(v) dv - \bar{v}^2 \right)^{1/2}, \quad (9)$$

and plot this against D_z , as shown in Figure 4. Overall this is a linear relation, but there is a strong dependence on v , creating large scatter. By taking the linear best fit we remove this dependence, essentially taking the uncertainty a galaxy would have if it had zero peculiar velocity. For our bulk flow estimation, we use the velocity uncertainty given by this linear best-fit:

$$\sigma_n = 0.324 H_0 D_z. \quad (10)$$

This approximation removes the dependence of the velocity uncertainty on the measured v . This is an important correction, because the weights assigned to each galaxy in the bulk flow estimation are derived depending on the galaxy's velocity uncertainty. If the weights were correlated with the velocities themselves, this would produce a biased bulk flow measurement, made worse if the redshift distribution of galaxies is not evenly distributed over the sky, as in 6dFGS.

4 BULK FLOW ESTIMATORS

The bulk flow is the average peculiar velocity in a given volume of space, usually taken to be a spherical region centred on us, and defined by

$$\mathbf{U}(R) = \frac{3}{4\pi R^3} \int_{x=0}^R \mathbf{v}(\mathbf{x}) d^3x, \quad (11)$$

where R is the radius of the sphere in which the bulk flow is measured. In practice however, we can never perfectly sample the velocity field. Peculiar velocity samples are typically sparse, with complicated geometries and large measurement uncertainties. Additionally, we only observe the line-of-sight component of the peculiar velocities.

Different bulk flow estimators have been suggested in the literature to account for this, including the maximum

likelihood estimate (Dressler et al. 1987b; Kaiser 1988), comparison with the density field (Bertschinger et al. 1990; Dekel et al. 1999; Willick & Strauss 1998; Turnbull et al. 2012; Magoulas et al. 2015), reconstruction of the velocity field based on a velocity power spectrum (Nusser & Davis 2011) and the so-called ‘Minimum Variance’ weighting method (Watkins et al. 2009; Feldman et al. 2010).

In this paper we apply the maximum likelihood estimate (MLE) and the Minimum Variance (MV) method to 6dFGSv. These both evaluate the bulk flow as a weighted sum of the peculiar velocities. Given a sample of objects with radial peculiar velocities v_n , these methods assign a weight $w_{i,n}$ corresponding to the i^{th} direction for each galaxy. The bulk flow $\mathbf{U} = (u_x, u_y, u_z)$ is then

$$u_i = \sum_n w_{i,n} v_n. \quad (12)$$

In the following two subsections we give an overview of these two weighting methods.

A parallel analysis of the 6dFGSv bulk flow is currently being made by Magoulas et al. (in prep), who apply a different bulk flow estimation method. They use forward modelling, performing a Maximum Likelihood fit to a bulk flow model transformed into the observational space of the Fundamental Plane parameters. This approach effectively fits the measured logarithmic distance ratios $\eta = \log(D_z/D_r)$ without converting to linear velocities, and can fully account for the (Gaussian) error distribution in the observational space.

4.1 Maximum likelihood estimate

The MLE has traditionally been the most common technique used to measure the bulk flow. We consider here the MLE using inverse variance weighting from Kaiser (1988). Given a sample of N objects at positions $r_{n,i}$, each having a measured line-of-sight velocity v_n with uncertainty σ_n , the MLE weight for the n^{th} galaxy is

$$w_{i,n} = \sum_j A_{ij}^{-1} \frac{\hat{r}_{n,j}}{\sigma_n^2 + \sigma_*^2} \quad (13)$$

where

$$A_{ij} = \sum_n \frac{\hat{r}_{n,i} \hat{r}_{n,j}}{\sigma_n^2 + \sigma_*^2}. \quad (14)$$

The parameter σ_* is the 1D velocity dispersion, usually assumed to be $\sim 300 \text{ km s}^{-1}$; we assume galaxies have random motions drawn from a Gaussian distribution with this dispersion, in addition to the bulk flow component. These random motions add to the noise for any given galaxy.

This solution makes a number of simplifying assumptions:

- (i) the observational errors, σ_n , are Gaussian
- (ii) linear theory holds, so $v_n \ll H_0 r_n$
- (iii) we can neglect uncertainty in r_n
- (iv) u_i is fairly insensitive to small-scale velocities, and that σ_* , which will be strongly influenced by nonlinear flows, can be fixed at a given value.

In practice, nearly all of these assumptions will be violated to some extent. The observational errors on v are *not* Gaussian, $v \sim 20\text{--}30\%$ of $H_0 r$, and linear theory does not strictly

apply, since $\sigma_* \sim 300 \text{ km s}^{-1}$ is comparable to the expected bulk flow amplitude on the scales we measure. However, we do not expect these to have a significant impact on our measurement. Since our analysis is done in redshift-space, the uncertainty on r_n is the uncertainty on the redshift distance, which is indeed negligible. We find that our result is insensitive to the choice of σ_* , which we discuss further in Section 4.4. We leave further analysis of non-Gaussian uncertainties to future work.

4.2 Minimum Variance method

Although the MLE is simple to perform, it has several disadvantages. It will have a complex window function dependent on the geometry and uncertainties of a particular survey, making it difficult to compare between surveys and with theory. It is also density-weighted rather than volume-weighted, as it tends to upweight high-density regions where galaxies are more likely to be measured, and down-weight low density regions. Finally, because it down-weights more distant galaxies which have larger uncertainties, the MLE tends to be dominated by the nearest galaxies in the sample and so minimises the scale on which the bulk flow is measured.

The ‘Minimum Variance’ (MV) method of Watkins et al. (2009) (hereafter WFH09) and Feldman et al. (2010) is an extension of the MLE method, which constructs a more optimal set of weights that allow a volume-weighted measurement of the bulk flow to be made with a specified window function. This is achieved by determining weights $w_{i,n}$ that minimise the variance between the bulk flow measured by the sample, and the bulk flow that would be measured by an ‘ideal’ survey, with the specified window function. In their case, they choose this to be a perfectly sampled, all-sky Gaussian survey with ‘ideal’ radius R_I .

While the MV method is more optimal than the MLE method, it still has some disadvantages. It is not necessarily an unbiased estimator, especially since it still assumes the velocity uncertainties are Gaussian, and it minimises the variance only on the particular quantity it tries to measure (i.e. the bulk flow of a given window function) rather than the bulk flow of the full dataset. However, it provides a much more optimal way of comparing the bulk flow in a survey with a theoretical model and with other surveys. Tests of its robustness using N -body simulations have shown that it correctly recovers the underlying bulk flow, and is unbiased by the survey geometry and nonlinear flows (Agarwal et al. 2012).

The MV weights are calculated from

$$\mathbf{w}_i = (\mathbf{G} + \lambda \mathbf{P})^{-1} \mathbf{Q}_i, \quad (15)$$

where i denotes the three bulk flow components. \mathbf{P} is the $k = 0$ limit of the angle-averaged window function, \mathbf{Q}_i incorporates information about the input ideal window function, λ is a Lagrange multiplier, and \mathbf{G} is the covariance matrix of the individual peculiar velocities, given by

$$\begin{aligned} G_{nm} &= \langle v_n v_m \rangle \\ &= \delta_{nm} (\sigma_n^2 + \sigma_*^2) + \frac{(f(\Omega_m, z) H_0 a)^2}{2\pi^2} \int P(k) f_{mn}(k) dk, \end{aligned} \quad (16)$$

where H_0 is the Hubble constant, $f \sim \Omega_m^{0.55}(z)$ is the growth

rate of cosmic structure, and $f_{mn}(k)$ is the angle-averaged window function,

$$f_{mn}(k) = \int \frac{d^2\hat{k}}{4\pi} (\hat{r}_n \cdot \hat{k})(\hat{r}_m \cdot \hat{k}) \times \exp[ik\hat{k} \cdot (\mathbf{r}_n - \mathbf{r}_m)]. \quad (17)$$

The first term in Equation 16 is the noise term, while the second part is the cosmic variance, or ‘geometrical’ term, and incorporates the power spectrum of a given cosmological model. Equation 17 can be calculated analytically, as shown in the appendix of Ma et al. (2011). Further details of how the weights are calculated are presented in Appendix A; also see WFH09 and Feldman et al. (2010).

Following WFH09 we also choose a Gaussian survey as our ideal survey, using two different ideal radii: (1) $R_I = 50 h^{-1} \text{Mpc}$ for comparison with WFH09; and (2) $R_I = 70 h^{-1} \text{Mpc}$. We choose the latter since it is close to the ‘Maximum Likelihood Estimate depth’ of 6dFGSv, which is calculated via

$$d_{\text{MLE}} = \frac{\sum r_n w_n}{\sum w_n}, \quad (18)$$

where the MLE weights are $w_n = 1/(\sigma_n^2 + \sigma_*^2)$. We find this to be $\sim 72 h^{-1} \text{Mpc}$ for 6dFGSv. This is the optimal depth for a bulk flow measurement in 6dFGSv.

The ideal Gaussian survey will have a radial density profile given by

$$\rho(r) \propto \exp(-r^2/2R_I^2), \quad (19)$$

and its radial number distribution is

$$N(r) \propto r^2 \exp(-r^2/2R_I^2). \quad (20)$$

We plot $N(r)$ for our two ideal surveys in Figure 5, along with the number distribution of 6dFGSv for comparison. The 6dFGSv sample has a cutoff at $160 h^{-1} \text{Mpc}$ corresponding to $z = 0.0537$, so we also apply this to our ideal surveys.

The ideal survey used by WFH09 is an all-sky survey, since the dataset they used was all-sky; in the case of 6dFGSv, we only have half the sky. We discuss the effect of partial sky coverage on our measurement in Section 6.

4.3 Bulk flow uncertainties

The covariance matrix of the bulk flow moments, R_{ij} , can be written as:

$$R_{ij} = \langle u_i u_j \rangle = \sum_{mn} w_{im} w_{jn} G_{mn} = R_{ij}^{(\epsilon)} + R_{ij}^{(v)}, \quad (21)$$

where $R_{ij}^{(\epsilon)}$ represents the noise contribution,

$$R_{ij}^{(\epsilon)} = \sum_n w_{i,n} w_{j,n} (\sigma_n^2 + \sigma_*^2), \quad (22)$$

and $R_{ij}^{(v)}$ represents the cosmic variance contribution,

$$R_{ij}^{(v)} = \frac{(f(\Omega_m, z) H_0 a)^2}{2\pi^2} \int_0^\infty dk \mathcal{W}_{ij}^2(k) P(k), \quad (23)$$

where $\mathcal{W}_{ij}^2(k)$ is the angle-averaged tensor window function,

$$\mathcal{W}_{ij}^2(k) = \sum_{n,m} w_{i,n} w_{j,m} f_{mn}(k). \quad (24)$$

The errors on the bulk flow moments, σ_i , are then $\sigma_i = \sqrt{R_{ii}}$, and the error on the bulk flow magnitude is $\sigma_U^2 = J R_{ij} J^T$, where J is the Jacobian of U , $\partial U / \partial u_i$.

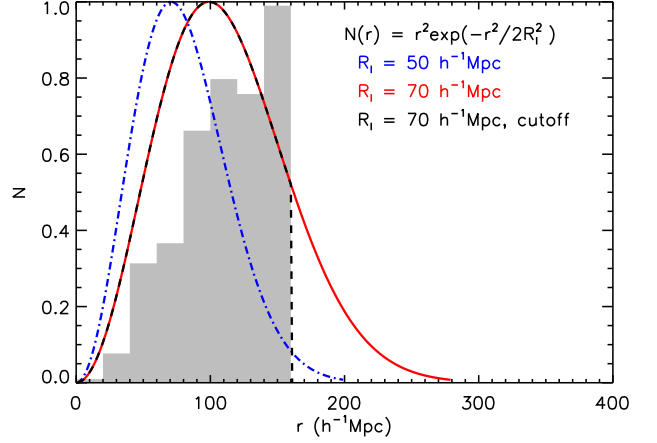


Figure 5. Radial number distribution $N(r)$ of the Gaussian filters we use for measuring the 6dFGSv bulk flow. The filters have (i) $R_I = 50 h^{-1} \text{Mpc}$ radius (blue dot-dashed line), (ii) $R_I = 70 h^{-1} \text{Mpc}$ radius (red solid line) and (iii) $R_I = 70 h^{-1} \text{Mpc}$ radius with a cutoff at $160 h^{-1} \text{Mpc}$, corresponding to the redshift cut of the data (black dashed). The distribution of the data is shown by the grey histogram for comparison.

4.4 σ_* estimation

The 1D velocity dispersion parameter σ_* , as previously mentioned, accounts for small-scale random motions. The value of σ_* affects the weights of nearby galaxies most strongly, since they have the smallest velocity errors, but in the Minimum Variance method where these are down-weighted by the ideal window function, σ_* will only have a small effect on the measured bulk flow (Feldman et al. 2010).

In the case of 6dFGSv, small-scale velocities need to be accounted for in the fitting of the FP, since the fitting is done assuming each galaxy is at its redshift distance, and so velocities add to the scatter of the plane. A value of $\sigma_* = 300 \text{ km s}^{-1}$ is accounted for in the fitting of the FP by M12 and S14, and is effectively subtracted from the uncertainty in the $P(\eta)$ distributions. This means we need to ‘add back in’ this uncertainty in our bulk flow weights. Johnson et al. (2014) perform a fit to σ_* for the 6dFGSv sample and find it to peak at zero. However, σ_* also acts to regularise the bulk flow weights, to prevent galaxies with low error dominating the results, so assuming a zero σ_* is not ideal. We find that varying σ_* from 0 to 250 km s^{-1} has little effect on our results, changing the MV bulk flow on the order of $\sim 2\%$. We therefore fix $\sigma_* = 250 \text{ km s}^{-1}$ for our analysis.

5 6dFGSv SELECTION FUNCTION AND ΛCDM MOCK CATALOGUES

In order to test possible systematics in our bulk flow measurement arising from the survey selection function, we apply our bulk flow analysis to ΛCDM mock catalogues of 6dFGSv, incorporating the survey selection function. To create ΛCDM peculiar velocity mocks, we need to make use of an N -body simulation which provides both the positions and

velocities of galaxies. In this section we describe how we determine the selection function of 6dFGSv, and use this to generate mock catalogues using the GigggleZ N -body simulation. This selection function also allows for the creation of random catalogues for clustering analysis.

5.1 6dFGSv survey selection function

The selection function $W(\mathbf{x})$ is a function indicating the expected number density of 6dFGSv galaxies at a position \mathbf{x} , due to the different selection criteria of the sample. These can be both angular- and redshift- dependent. To implement the selection function in our mocks, we reproduce the selection process described in M12 and S14 to obtain the 6dFGSv sample of 8,885 galaxies from the full 6dFGS redshift sample of 125,000 galaxies. In summary, they first select galaxies suitable for fitting the FP, by choosing galaxies with reliable redshifts (with redshift quality $Q = 3 - 5$) and redshifts less than $16\,500\text{ km s}^{-1}$ (or $z < 0.0537$), above which a key spectral feature used to measure velocity dispersion is shifted out of the wavelength range. They then morphologically select early-type (E/S0) galaxies, by matching the observed spectra to template galaxy spectra. This produced a sample of $\sim 20\,000$ galaxies.

These $\sim 20\,000$ galaxies then had their velocity dispersions measured using the Fourier cross-correlation technique (Campbell 2009). Of these, galaxies with a signal-to-noise $S/N > 5\text{Å}^{-1}$, and velocity dispersions larger than the instrumental resolution limit ($s \geq 2.05$, or $\sigma_0 \geq 112\text{ km s}^{-1}$) were selected, to produce a ‘Fundamental Plane sample’ of 11 287 galaxies. This sample, with both spectroscopic measurements from 6dFGS and photometric measurements from 2MASS in the J , H and K bands, was used by M12 for the fitting of the FP parameters.

Finally, the peculiar velocity sample 6dFGSv was obtained from the FP sample after several further cuts. A stricter redshift limit of $cz < 16120$ ($z < 0.0537$) was imposed in the CMB frame, along with further magnitude cuts of $J \leq 13.65$, $H \leq 12.85$ and $K \leq 12.55$, to maintain high completeness over the sky. Further galaxies were removed after a visual inspection, and a velocity dispersion χ^2 cut, to obtain the final peculiar velocity sample of 8885 galaxies.

5.2 Fundamental Plane fitting

Here we introduce the FP terminology we will use in making the mocks - see M12 for further details. The FP relation can be written in logarithmic units as

$$r = as + bi + c, \quad (25)$$

where $r \equiv \log R_e$, $s \equiv \log \sigma_0$ and $i \equiv \log \langle I_e \rangle$, where R_e is the effective radius in units of $h^{-1}\text{ kpc}$, σ_0 is the central velocity dispersion in units of km s^{-1} , and $\langle I_e \rangle$ is the mean surface brightness, in units of $L_\odot\text{ pc}^{-2}$. The coefficients a and b are the slopes of the plane and c is the offset of the plane. M12 use logarithms of base 10.

M12 determine the FP parameters for 6dFGSv using a maximum-likelihood fit to a 3D Gaussian model. The FP can be described either in terms of the observational parameters (r, s, i), or in terms of the three unit vectors corresponding to

the axes of the 3D Gaussian describing the galaxy distribution. M12 refer to these as ‘FP-space’ and ‘ \mathbf{v} -space’ respectively. The model can then be described by eight parameters: $\{a, b, \bar{r}, \bar{s}, \bar{i}, \sigma_1, \sigma_2, \sigma_3\}$, where $(\bar{r}, \bar{s}, \bar{i})$ define the centre of the 3D Gaussian in FP-space and $(\sigma_1, \sigma_2, \sigma_3)$ are the dispersion of the Gaussian along each of the three axes in \mathbf{v} -space. The offset of the FP can be calculated as $c = \bar{r} - a\bar{s} - b\bar{i}$.

5.3 Mock sample algorithm

We create mock Λ CDM realisations of the 6dFGSv dataset for the set of FP parameters $\{a, b, c, \bar{r}, \bar{s}, \bar{i}, \sigma_1, \sigma_2, \sigma_3\}$ derived by M12. We use the following steps to reproduce the 6dFGSv selection function and generate the mock catalogue:

(i) For a Λ CDM mock, start by drawing haloes from an N -body simulation in a mass range equivalent to the 6dFGS elliptical galaxies, i.e. pick haloes that match the bias of 6dFGS (this is effectively a cut in morphological type).

Angular & Redshift cuts

(ii) Define the location of the observer, and calculate RA, Dec, true comoving distance D_r and radial peculiar velocity v for each galaxy. Also calculate the true and observed redshifts z_r, z , using Equation 4.

(iii) Only include haloes within hard angular cuts $\text{Dec} < 0^\circ$ and Galactic latitude $|b| > 10^\circ$.

(iv) Impose a redshift cut of $cz < 16\,120\text{ km s}^{-1}$.

(v) Normalise by applying a random subsampling to obtain the number of galaxies in the 6dFGS parent redshift sample.

Magnitude & Velocity Dispersion cuts

(vi) For each galaxy, draw values for v_1, v_2 and v_3 at random from a 3D Gaussian with standard deviations σ_1, σ_2 and σ_3 as listed in Table 3 of M12. We use the J-band values as the J-band has the smallest photometric errors.

(vii) Transform these values from the \mathbf{v} -space (principle axes) coordinate system to the $\{\mathbf{r}, \mathbf{s}, \mathbf{i}\}$ -space (observed parameters) coordinate system using the inverse of Equation 6 in M12, with the specified FP slopes (a and b) and FP mean values $(\bar{r}, \bar{s} \text{ and } \bar{i})$. This gives the true Fundamental Plane parameters (r_t, s_t, i_t) for the simulated galaxies.

(viii) Re-order each set of (r_t, s_t, i_t) parameters in descending order of luminosity,

$$\log L = l = 2r + i, \quad (26)$$

and assign them to the haloes in descending order of maximum circular velocity $V_{\text{max,sub}}$.

(ix) Use the comoving distance D_r of each galaxy from the observer to determine the angular radius θ from the physical radius r_t , by calculating the angular diameter distance D_A :

$$D_A \equiv \frac{r_t}{\theta} = \frac{D_r}{1 + z_{\text{true}}} \quad (27)$$

(this relation is true for $\Omega_k = 0$, see Hogg 1999). Then θ is obtained from

$$\log \theta = \log r_t - \log D_A. \quad (28)$$

(x) Determine the true apparent magnitude m_t from the angular radius θ and the *degraded* surface brightness i using

$$m_t = \langle \mu_e \rangle - 2.5 \log[2\pi\theta^2], \quad (29)$$

where $\langle \mu_e \rangle = M - 2.5i + 21.57$, where $M = 3.67$ for the J -band. The surface brightness i is first degraded by ‘de-correcting’ for K-correction and surface brightness dimming.

(xi) Obtain the correlated measurement uncertainties in r , s and i , $(\epsilon_r, \epsilon_s, \epsilon_i)$, from the magnitude m_i , using the matrix in Equation 13 of M12.

(xii) Add these measurement errors to $\{r, s, i\}$ to obtain the observed values $\{r_o, s_o, i_o\}$ for each galaxy.

(xiii) Only include galaxies with velocity dispersion $s_o > \log(116 \text{ km/s})$. (Cut for instrumental resolution).

(xiv) Determine the observed magnitude m_o using the observed values r_o and i_o .

(xv) Keep the galaxy if the observed magnitude m_o is brighter than the faint limit for the velocity sample ($J \leq 13.65$).

(xvi) Use the selection function described in Jones et al. (2006) to determine the angular completeness of the 6dFGS spectroscopic follow-up, given the (RA, Dec, m_o) values for each galaxy. Sub-sample the galaxies with this probability.

(xvii) Apply a random subsampling to account for cuts in signal-to-noise (S/N) ratio and R .

5.4 The Mocks

In order to generate Λ CDM mocks, we apply our mock sample algorithm to the GiggleZ (Giga-parsec WiggleZ) simulation. GiggleZ (Poole et al. 2014) is a suite of dark matter N -body simulations run at Swinburne University of Technology. It has a WMAP-5 cosmology with $(\Omega_\Lambda, \Omega_m, \Omega_b, h, \sigma_8, n) = (0.727, 0.273, 0.0456, 0.705, 0.812, 0.960)$. We use the GiggleZ Main simulation, which contains 2160^3 dark matter particles in a periodic box of side $1h^{-1}\text{Gpc}$. The particle mass is $7.5 \times 10^9 h^{-1} M_\odot$, which allows bound systems with masses $\gtrsim 1.5 \times 10^{11} h^{-1} M_\odot$ to be resolved.

Halo finding for GiggleZ was performed using SUBFIND (Springel et al. 2001), which utilises a friends-of-friends (FoF) algorithm to identify coherent overdensities of particles and a substructure analysis to determine bound overdensities within each FoF halo. We place a galaxy at the centre of each subhalo, and rank-order them by their maximum circular velocity ($V_{\text{max,sub}}$) to obtain the largest haloes, in order to reproduce the bias of the 6dFGSv sample.

We have generated 20 independent mocks of 6dFGSv within the GiggleZ volume. We show the mean and variance of the redshift distribution of our 20 mocks, compared with 6dFGSv, in Figure 6. The mocks appear higher than the data in the highest redshift bins ($0.04 < z < 0.05$), although this could possibly be attributed to cosmic variance. However, the large-scale bulk flow properties of the mocks will not depend strongly on the exact shape of the redshift distributions, since the bulk flow depends to first order on the velocities of galaxies, not on their number density.

6 RESULTS AND DISCUSSION

We present in this section the bulk flow results of our 6dFGSv analysis, for the MV and MLE estimators, along with the bulk flow results for our Λ CDM mocks. We then compare our results to a theoretical Λ CDM prediction,

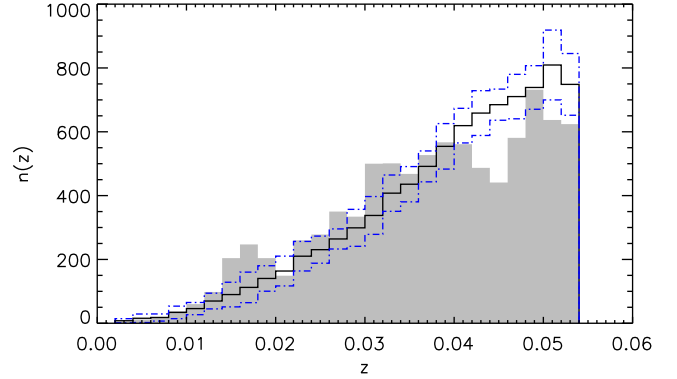


Figure 6. The mean redshift distribution of our 20 GiggleZ mocks (black histogram), along with the standard deviation (blue dot-dashed histogram), compared to 6dFGSv (solid grey histogram).

firstly considering the 3D bulk flow amplitude, and secondly considering each of the three 1D bulk flow components, to obtain constraints on Ω_m and σ_8 .

6.1 Bulk flow results

We have calculated the bulk flow for 6dFGSv, for the two different bulk flow estimators described in Section 4:

- (i) The Minimum Variance (MV) estimate, using two different ideal surveys: (1) a Gaussian survey with effective radius $R_I = 50 h^{-1} \text{Mpc}$, (2) a Gaussian survey of radius $R_I = 70 h^{-1} \text{Mpc}$. To each ideal survey we apply a cut-off at $160 h^{-1} \text{Mpc}$, the survey limit.
- (ii) The Maximum Likelihood Estimate (MLE).

Our measurement represents an estimation of the bulk flow in the southern hemisphere, out to $50 - 70 h^{-1} \text{Mpc}$.

The results are presented in Table 1, in both Galactic Cartesian coordinates and Equatorial Cartesian coordinates. We include the Equatorial coordinates, since 6dFGSv covers only half the sky in the Equatorial z direction (i.e. the southern hemisphere), and we would therefore expect increased variance in this direction; we wish to make any such effect clearly distinguishable. We may expect a smaller variance in the x and y directions. The uncertainties quoted are the noise uncertainties, with cosmic variance in parentheses. The cosmic variance is predicted for a given Λ CDM power spectrum, as we discuss further in Section 6.4.

For the MV estimator with $R_I = 50 h^{-1} \text{Mpc}$, we find a bulk flow amplitude of $|\mathbf{U}| = 248 \pm 58 \text{ km s}^{-1}$ in the direction $(l, b) = (318^\circ \pm 20^\circ, 40^\circ \pm 13^\circ)$, and for $R_I = 70 h^{-1} \text{Mpc}$, we find a bulk flow amplitude of $|\mathbf{U}| = 243 \pm 58 \text{ km s}^{-1}$ in the direction $(l, b) = (318^\circ \pm 20^\circ, 39^\circ \pm 13^\circ)$.

For the MLE, we find a bulk flow of $|\mathbf{U}| = 295 \pm 48 \text{ km s}^{-1}$ in the direction $(l, b) = (59^\circ \pm 36^\circ, 74^\circ \pm 11^\circ)$, which is not consistent with the direction of the MV results. The difference is largest in the Equatorial z direction, and we can see why from looking at the window function \mathcal{W}_{ii}^2 of the different estimators,

Table 1. Bulk flow results for the MV and MLE estimators, assuming peculiar velocity uncertainties $\sigma_n = 0.324H_0 D_z \text{ km s}^{-1}$ for each galaxy. Columns are the bulk flow magnitudes $|\mathbf{U}|$, the vector components (u_x, u_y, u_z) , and angular coordinates. The top panel shows Galactic coordinates, with angles in Galactic longitude (l) and latitude (b), while the lower panel shows Equatorial coordinates, with angles in Right Ascension (RA) and Declination (Dec). The uncertainties quoted are noise, with the cosmic variance uncertainty in parentheses. The MV methods use an ideal Gaussian window function, with radius $R_I = 50h^{-1} \text{ Mpc}$ or $R_I = 70h^{-1} \text{ Mpc}$, and with a cut-off at $160h^{-1} \text{ Mpc}$ corresponding to the redshift cut-off of the survey.

Bulk flow estimator	$ \mathbf{U} $ (km s^{-1})	u_x (km s^{-1})	u_y (km s^{-1})	u_z (km s^{-1})	l / RA ($^\circ$)	b / Dec ($^\circ$)
<i>Galactic coordinates</i>						
MV ($R_I = 50h^{-1} \text{ Mpc}$)	$248 \pm 58(100)$	$142 \pm 66(106)$	$-127 \pm 72(114)$	$159 \pm 59(103)$	318 ± 20	40 ± 13
MV ($R_I = 70h^{-1} \text{ Mpc}$)	$243 \pm 58(101)$	$139 \pm 66(106)$	$-125 \pm 72(114)$	$154 \pm 59(102)$	318 ± 20	39 ± 13
MLE	$295 \pm 48(138)$	$43 \pm 56(130)$	$72 \pm 52(165)$	$283 \pm 47(129)$	59 ± 36	74 ± 11
<i>Equatorial coordinates</i>						
MV ($R_I = 50h^{-1} \text{ Mpc}$)	$248 \pm 58(100)$	$-208 \pm 55(96)$	$-99 \pm 63(101)$	$-91 \pm 77(125)$	205 ± 16	-21 ± 17
MV ($R_I = 70h^{-1} \text{ Mpc}$)	$243 \pm 58(101)$	$-203 \pm 55(95)$	$-97 \pm 63(100)$	$-90 \pm 78(124)$	205 ± 16	-22 ± 18
MLE	$295 \pm 48(138)$	$-212 \pm 46(114)$	$-125 \pm 55(115)$	$162 \pm 53(186)$	211 ± 13	33 ± 10

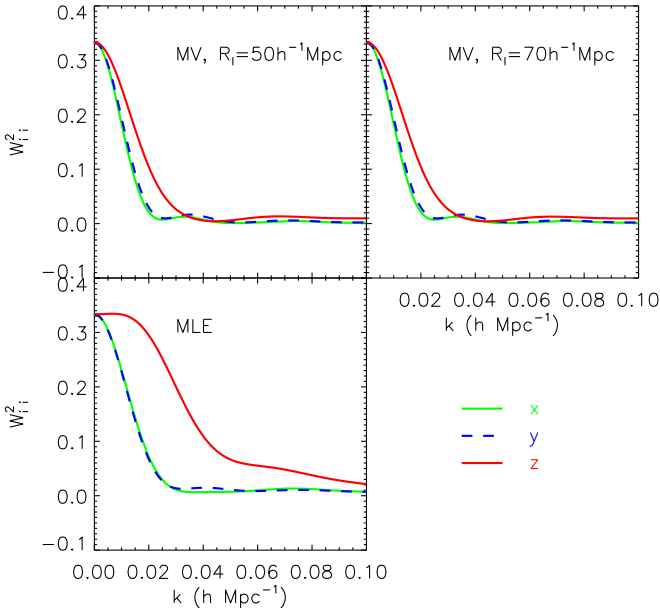


Figure 7. The window functions \mathcal{W}_{ii}^2 (from Eq. 24) of the bulk flow components for 6dFGSv, for each of our three estimators: the MV estimate with $R_I = 50$ or $R_I = 70h^{-1} \text{ Mpc}$, and the MLE method. The Equatorial Cartesian x, y, z components are the solid green, dashed blue, and solid red lines, respectively.

calculated from Eq. 24, in Figure 7. While the x and y window functions are similar for all the estimators, the z window function is less compact for the MLE, giving more weight to smaller scales.

We wish to clarify that the MV and MLE methods are different estimators of the bulk flow, and do not necessarily have to agree. They are based on different weightings over the volume, hence their different window functions, and so are quite free to give different results for both the amplitude and direction of the bulk flow. The MLE is much more sensitive to the window function of the survey than the MV, since the MV upweights a specified scale, while the scale of the MLE depends on the number of galaxies, their distribution, and their uncertainties. The 6dFGSv survey covers

only half the range of scales in the Equatorial z direction (i.e. the north-south direction) than the x and y directions (i.e. east-west), and so smaller scales contribute to the MLE bulk flow in the z direction. This is why the MLE window function is less compact in the z -direction. There is significant variance in the small-scale 6dFGSv velocity field, as shown by S14, so a difference in window function can give quite a large difference in the bulk flow, which is what we observe. What is important is how we compare the results with a theoretical model. The MV method is more straightforward to compare with theory, since it gives the bulk flow for a specified window function which we can include in the theoretical model.

We show the sky positions of our MV and MLE bulk flow measurements in Figure 8. The CMB dipole is shown for comparison, along with a number of recent bulk flow measurements from the literature. We also show on this plot the position of the Shapley Supercluster ($l = 312^\circ, b = 31^\circ$). Our MV measurement is very close to the direction of Shapley, and consistent with it within the angular uncertainties. Unlike all-sky peculiar velocity surveys, 6dFGSv will be dominated by southern-sky structures, since the gradient of the velocity field towards these structures will be larger, and so it is not surprising that our measurement is close to Shapley. Also, the 6dFGSv number density of galaxies peaks beyond $100h^{-1} \text{ Mpc}$, incorporating part of Shapley, so this survey selection criteria itself will likely cause the Shapley region to dominate our bulk flow results.

In this figure, we also show the bulk flow results from our 20 GigggleZ-based mock catalogues, which we will discuss further in Section 6.2.

6.2 6dFGSv bulk flow distribution in ΛCDM mocks

We use our N -body simulation-based mock catalogues to determine the expected distribution of bulk flows for 6dFGSv in a ΛCDM universe. We calculate the bulk flow amplitude in each of the 20 mocks, using the MV method with $R_I = 50h^{-1} \text{ Mpc}$, and show their histogram in Figure 9. We also show the corresponding bulk flow magnitude from the data, along with the 1σ noise uncertainty; this is above the average, but within the expected range of the mocks. Seven

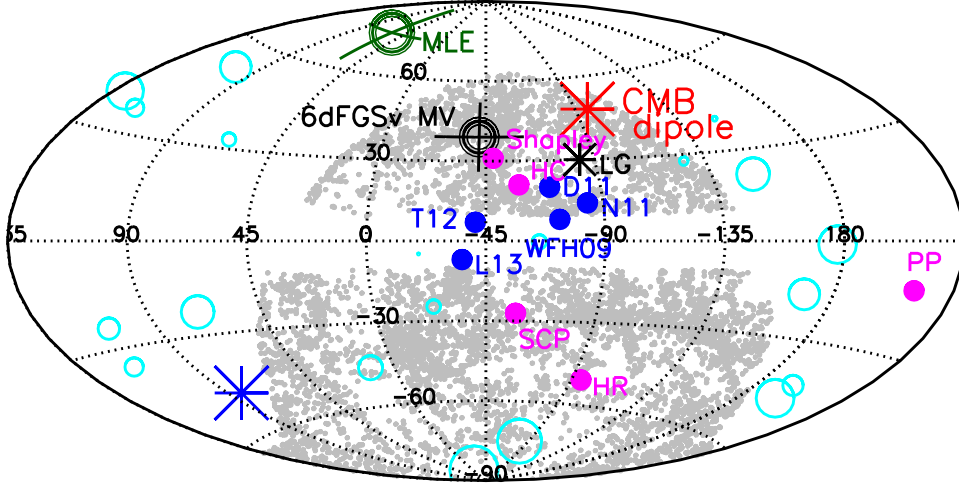


Figure 8. The 6dFGSv bulk flow result in this work, compared with other bulk flow measurements and nearby superclusters. The figure shows Galactic longitude (l) and latitude (b), in an Aitoff projection. Our MV result for $R_I = 70h^{-1}$ Mpc is shown as the black circle, while our MLE result is shown as the green circle (labelled). The diameter of the circles is proportional to the amplitude of the bulk flow, with inner and outer circles indicating the 1σ confidence interval of this amplitude. The error bars show the 1σ angular uncertainty. The cyan circles show the distribution of bulk flows measured in our 20 GiggleZ 6dFGSv mock catalogues. Again, the size of the circles corresponds to the bulk flow amplitude, and since these are from simulations they have no measurement uncertainties. Our result for $R_I = 50h^{-1}$ Mpc is almost identical to the one for $70h^{-1}$ Mpc. The 6dFGSv galaxies are shown in grey for reference. We show the directions of several other results from the literature by the solid blue circles: WFH09 (W09), Dai et al. (2011) (D11), Nusser & Davis (2011) (N11), Turnbull et al. (2012) (T12), Lavaux et al. (2013) (L13) and Planck Collaboration et al. (2014b) (P13). The four largest local superclusters are shown by the solid magenta circles: the Shapley Supercluster, Hydrus-Centaurus (HC), Horologium-Reticulum (HR) and Perseus-Pisces (PP). The South Celestial Pole (SCP) is also shown in magenta for reference. The CMB dipole is indicated by the red and blue stars (with red the direction of the dipole), and the direction of the Local Group motion (from Kogut et al. 1993) is shown by the black star.

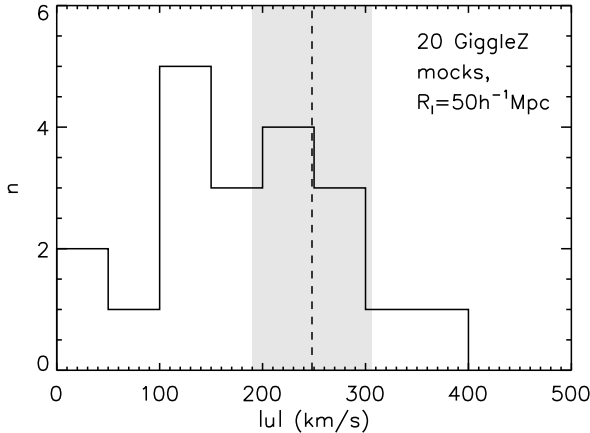


Figure 9. Histogram of the bulk flow amplitudes $|U|$ in our 20 GiggleZ-based 6dFGSv mocks, for the MV estimator with $R_I = 50h^{-1}$ Mpc. The vertical dashed line shows the corresponding amplitude for the data, and the grey shaded area indicates the 1σ noise uncertainty in the measurement.

of the mocks, or 35%, lie above our result, while 65% lie below.

The direction and amplitude of the bulk flow measured in each of these mocks is shown in Figure 8. This is a useful test to see whether the survey window function can bias

the direction of the measured bulk flow. We see that the directions of the mocks appear fairly random and isotropic. There are more in the northern sky (13) than the southern sky (7), but this is not significant. It is also possible the mocks may share large-scale modes, since they all lie within the same Gpc volume, so it could be they are not completely independent.

6.3 Comparison with linear theory: 3D bulk flow

Since the bulk flow amplitude is sensitive to the large-scale modes of the matter power spectrum, the measured bulk flow can be compared with the predicted value for a given cosmological model. If the Universe is statistically homogeneous and isotropic, then the expected mean bulk flow at any location is zero. The root-mean-square (RMS) variance of the bulk flow amplitude, however, is cosmologically interesting, since it depends on the matter power spectrum, as well as the scale and window function in which it is measured.

We compare our 6dFGSv MV bulk flow amplitude, for both our ideal survey radii, to a Λ CDM linear-theory prediction in Figure 10. This prediction is the most likely bulk flow amplitude, $V_{ML}(R)$, which depends on the RMS velocity dispersion, σ_V . The RMS velocity dispersion is given by

$$\sigma_V^2(R) \equiv \langle V(R)^2 \rangle = \frac{H_0^2 f^2}{2\pi^2} \int_{k=0}^{\infty} dk P(k) \widetilde{W}(k; R)^2, \quad (30)$$

where $P(k)$ is the matter power spectrum, and $\widetilde{W}(k; R)$ is

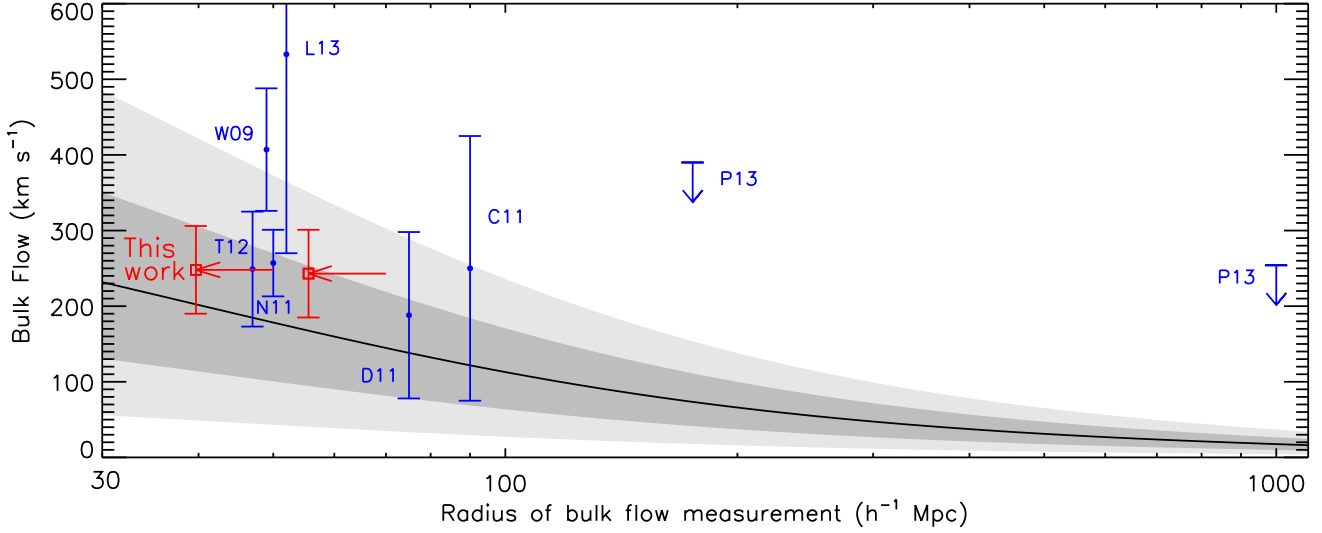


Figure 10. The 6dFGSv bulk flow results in this work (red squares with error bars) for the MV method with radius $R_I = 50$ and $70 h^{-1}$ Mpc, compared to a Λ CDM prediction. These results are plotted at ‘effective radii’, corresponding to the radius of a full sphere with the same volume as the half-sky measurement, to show the variance we actually expect. The red arrows show how far we have shifted the points from the measured radii R_I to the effective radii R_{eff} . The black solid curve is a linear-theory Λ CDM prediction for an all-sky Gaussian window function. The dark grey and light grey regions show the 68.3% and 95.5% confidence levels, assuming a Maxwellian distribution of velocities. Other recent measurements are shown in blue – these are: Lavaux et al. (2013) (L13), WFH09 (W09), Turnbull et al. (2012) (T12), Colin et al. (2011) (C11), Planck Collaboration et al. (2014b) (P13), Dai et al. (2011) (D11), and Nusser & Davis (2011) (N11). Several of these results - C11, D11, N11 and P13 - have top hat windows, and so we plot them at half their quoted radius, to be more comparable to the characteristic radius of the Gaussian window prediction. All error bars are 1σ , while the two Planck arrows are the 95% upper limits.

the Fourier Transform of the window function, $W(R)$, at effective radius R . In this plot, we use an all-sky Gaussian window function, $\tilde{W}_G = \exp(-k^2 R^2/2)$. (In the next section, we will use the exact window function of the survey to perform cosmological fits.)

The expected bulk flow velocity $V(R)$ can be predicted from σ_V , assuming the peculiar velocity field is Maxwellian, which it will be if the density field is Gaussian random. For a Maxwellian distribution, the probability distribution function of the bulk flow amplitude V is (Bahcall et al. 1994; Coles & Lucchin 2002)

$$p(V)dV = \sqrt{\frac{2}{\pi}} \left(\frac{3}{\sigma_V^2} \right)^{3/2} V^2 \exp\left(-\frac{3V^2}{2\sigma_V^2}\right) dV. \quad (31)$$

For such a distribution the most likely (maximum likelihood) bulk flow amplitude is $V_{\text{ML}} = \sqrt{2/3} \sigma_V$, while the expectation value is $\langle V \rangle = 2V_{\text{ML}}/\sqrt{\pi} = \sqrt{8/3\pi} \sigma_V$.

In Figure 10 we plot V_{ML} along with the upper and lower 1σ and 2σ confidence levels as the dark and light grey shaded regions, found from integrating Equation 31. These confidence levels correspond to the variance ranges $V_{\text{ML}}^{+0.419\sigma_V}_{-0.356\sigma_V}$ (1σ) and $V_{\text{ML}}^{+0.891\sigma_V}_{-0.619\sigma_V}$ (2σ). To calculate σ_V , we use a Λ CDM matter power spectrum, generated using CAMB (Lewis et al. 2000) with nonlinear evolution calculated using HALOFIT (Smith et al. 2003), and with the parameters listed in Section 1.

Caution is needed in interpreting this plot, since the different surveys have different window functions, and so cannot be directly compared, either with each other or with the theoretical prediction for a perfect all-sky Gaussian. A selection function tends to reduce the effective scale of a survey,

which increases σ_V and hence V for that survey. However, simulations show that the PDFs of bulk flows depend primarily on σ_V , and not on the type of window function, and so assuming an effective radius for the window function used in the model (e.g. a Gaussian in our case) that reproduces the same σ_V as the survey window function would allow a comparison at that scale (Li et al. 2012). We have not done this in this plot, and note that there is some uncertainty on the effective scale of the different surveys.

Since 6dFGSv only covers half the sky, we would expect our measurements at given radius R_I to have more cosmic variance than predicted by the full-sky model at this radius. Conversely, we could consider 6dFGSv to be at a smaller effective radius. We therefore plot our 6dFGSv MV results at ‘effective radii’ R_{eff} accounting for the fact that 6dFGSv covers only half the sky. For each of the $R_I = 50$ and $R_I = 70 h^{-1}$ Mpc results, we calculate the radius of a full sphere with the same volume as the half-sky measurement, i.e.

$$R_{\text{eff}} = (R_I^3/2)^{1/3}. \quad (32)$$

This gives effective radii of $R_{\text{eff}} = (39.7, 55.6) h^{-1}$ Mpc for the $R_I = (50, 70) h^{-1}$ Mpc measurements. We plot arrows showing how we have shifted the measurements from R_I to R_{eff} . However, since 6dFGSv is not a perfectly sampled hemisphere, we might expect the effective radii to be even smaller than the R_{eff} we calculate.

From Figure 10 we see that once shifted to the effective radii, both the 6dFGSv $R_I = 50 h^{-1}$ Mpc and $R_I = 70 h^{-1}$ Mpc bulk flow results appear to be consistent within 68.3% confidence with the theoretical prediction.

The uncertainty on the effective radii of previous sur-

veys may mean that those that showed higher than predicted bulk flows could have been compared to theory at too large a radius, without accounting for how the window function reduces the effective volume of the survey. It would be illuminating to recalculate the effective radii of these surveys to investigate this; we leave this for future work.

6.4 Comparison with linear theory: 1D bulk flow

Unlike the 3D bulk flow amplitude, the 1D bulk flow components u_i are Gaussian-distributed, making them more useful for a robust test of Λ CDM. The 1D RMS velocity variance is given for a particular survey by the covariance matrix of the bulk flow moments, R_{ij} , which we defined in section 4.3. It is the sum of a noise component and a cosmic variance component, and it depends on the survey geometry, the measurement noise, and the matter power spectrum. It is very similar to the RMS velocity variance σ_V in Equation 30, except for the addition of the noise component, and the cosmic variance component $R_{ij}^{(v)}$ contains the tensor window function $\mathcal{W}_{ij}(k)$. (We previously defined σ_* as the 1D velocity variance; this is in principle the average variance over all scales, which we assumed to be equal to $\sim 250 \text{ km s}^{-1}$. Here, however, we are looking at the variance as a function of scale.)

The deviation from zero of the observed bulk flow components u_i can be directly compared with the predicted dispersion, by calculating the χ^2 for the three moments,

$$\chi^2 = \sum_{i,j} u_i R_{ij}^{-1} u_j, \quad (33)$$

where i and j both go from 1 to 3 to specify the bulk flow components, u_i and u_j are the measured bulk flow components, and R_{ij} is the covariance matrix of the moments for a specified set of cosmological parameters.

R_{ij} is dominated by the cosmic variance term, typically of order $\sim 100 \text{ km s}^{-1}$, while the noise term is typically $\sim 40 \text{ km s}^{-1}$. Since the bulk flow depends on large-scale density fluctuations, R_{ij} will be most sensitive to the amplitude and shape of the power spectrum. The power spectrum amplitude is parameterised by the RMS density fluctuations in spheres of $8h^{-1} \text{ Mpc}$ radius, σ_8 , while the shape is parameterised by the shape parameter, Γ , which on large scales can be approximated by $\Gamma = \Omega_m h$. The dependence on Ω_m also comes into the $f(\Omega_m, z)^2$ factor. We therefore follow WFH09 in using the bulk flow to constrain a combination of Ω_m and σ_8 – in our case, we fix h to the best-fit value from *Planck*, $h = 0.67$.

In order to fit Ω_m and σ_8 we use the likelihood, following WFH09, which is given by

$$\mathcal{L}(\Theta) \propto \frac{1}{\sqrt{|R|}} \exp \left(-\frac{1}{2} u_i R_{ij}^{-1} u_j \right), \quad (34)$$

where Θ is the vector of parameters. In our case, $\Theta = (\Omega_m, \sigma_8)$, and we fix all other parameters to their *Planck* values.

We show our constraints on σ_8 and Ω_m for our MV results in Figure 11. There is a degeneracy between σ_8 and Ω_m , since a lower σ_8 requires a lower Ω_m to produce the same bulk flow; or, for fixed σ_8 , lower values of Ω_m lead to a larger bulk flow. This is because if σ_8 is fixed, then a lower

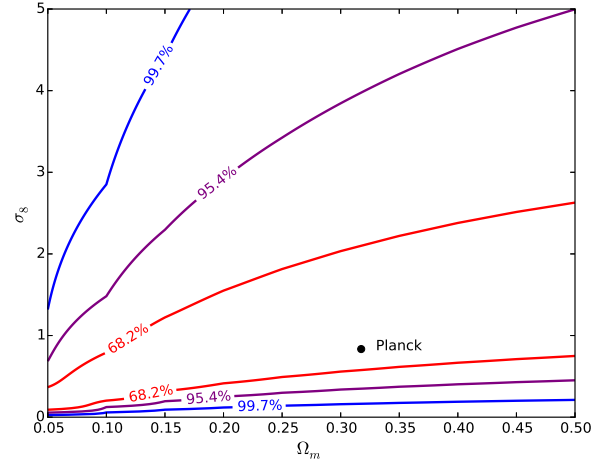


Figure 11. The likelihood-based confidence levels on Ω_m and σ_8 , obtained from the 6dFGSv MV bulk flow measurement with $R_I = 70 h^{-1} \text{ Mpc}$. The black point indicates the best fit values found by *Planck*, used as the fiducial values in this work. The result for $R_I = 50 h^{-1} \text{ Mpc}$ is very similar to this plot.

Ω_m requires a larger power spectrum amplitude on large scales to allow this normalisation. However, since a lower Ω_m also decreases the growth rate $f(\Omega_m, z)$, these two effects partially cancel, and so the bulk flow does not have much constraining power on Ω_m . The *Planck* value is shown as the black point, and is within the 1σ range of our measurement.

Marginalising over Ω_m , we obtain the likelihood for σ_8 . The results are shown in Figure 12. Our results favour a high value of σ_8 , but we do not find a significant disagreement with Λ CDM. For the MV $R_I = 50 h^{-1} \text{ Mpc}$ measurement, we find $\sigma_8 = 1.03^{+1.08}_{-0.58}$ (68.27% C.L.), and for $R_I = 70 h^{-1} \text{ Mpc}$, we find $\sigma_8 = 1.01^{+1.07}_{-0.58}$. Both of these are consistent with the *Planck* value of 0.83 ± 0.03 (Planck Collaboration et al. 2014a).

The diagonal elements of R_{ij} provide the expected 1D RMS bulk flow variance $\sigma_{V,i}^2$ in each of the three directions i , for a given survey window function and model power spectrum. Following WFH09, we list $\sigma_{V,i} = \sqrt{R_{ii}}$ in Table 2 for 6dFGSv, for the MLE and MV estimators.

We also show in this table the 1D and 3D RMS velocities calculated from our 20 GiggleZ-based mocks, using the MV estimator with $R_I = 50 h^{-1} \text{ Mpc}$. We would expect these to closely agree with the 6dFGSv results for $R_I = 50 h^{-1} \text{ Mpc}$, since the mocks reproduce the window function of the data, and this is roughly true. The last two rows of Table 2 show the analytic prediction for an all-sky Gaussian window function with radius 50 or $70 h^{-1} \text{ Mpc}$, by evaluating Equation 30 at these values of R .

6.5 Bulk flow in redshift shells

It is interesting to look at how the bulk flow varies as a function of redshift. In Figure 13 we plot the MLE bulk flow, split into redshift bins of $\Delta z = 0.01$. In each redshift bin, we re-calculate the MLE weights for only galaxies in that bin. The results are noisy, but the amplitude of the bulk flow seems to be fairly constant up to the maximum

Table 2. Comparison of the expected 1D RMS velocity $\sigma_{V,i}$, and 3D RMS velocity σ_V , for 6dFGSv, our GigggleZ-based 6dFGSv mocks, and for theory. We use Equatorial Cartesian coordinates, and assume a Λ CDM cosmology with parameters listed in Section 1.

Source & R_I (h^{-1} Mpc)	$\sigma_{V,x}$ (km s^{-1})	$\sigma_{V,y}$ (km s^{-1})	$\sigma_{V,z}$ (km s^{-1})	σ_V (km s^{-1})
6dFGSv: ^a				
MLE ($R_I \sim 70$)	122	122	193	139
MV, $R_I = 50$	95	100	122	101
MV, $R_I = 70$	95	100	123	102
Mocks: ^b				
MV, $R_I = 50$	129	114	120	210
Theory: ^c				
\widehat{W}_G , $R_I = 50$	-	-	-	218
\widehat{W}_G , $R_I = 70$	-	-	-	177

^a $\sigma_{V,i} = \sqrt{R_{ii}}$, from Eq. 21, and $\sigma_V^2 = J R_{ij} J^T$, where J is the Jacobian. Includes both noise and cosmic variance.

^b All calculated from root mean square of bulk flow components of 20 mocks. Includes both noise and cosmic variance.

^c Calculated from Eq. 30. Includes noise only and assumes a full-sky window function.

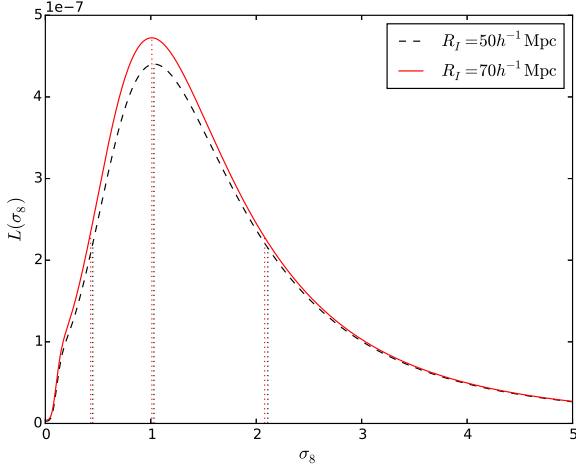


Figure 12. Likelihood of the value of σ_8 from our bulk flow measurement, after marginalising over Ω_m . The black dashed curve is for the MV $R_I = 50 h^{-1}$ Mpc measurement, and the red curve is for $R_I = 70 h^{-1}$ Mpc. The dotted lines indicate the maximum of the likelihood and 68.27% confidence levels.

redshift of $z = 0.054$. This is what would be expected if the source of the bulk flow is an overdensity more distant than the scales measured.

6.6 Zero-point uncertainty

So far our analysis has assumed a fixed zero-point for the Fundamental Plane. Springob et al. (2014) fix the zero-point by assuming zero average radial peculiar velocity in a ‘great circle’ around the equator, consisting of 3828 galaxies with $-20^\circ \leq \text{Dec} \leq 0^\circ$. (In practice they assume zero average logarithmic distance ratio η). However, this zero-point estimation has both statistical uncertainty and cosmic variance. We investigate the effect of these on our bulk flow measurement here.

The statistical uncertainty on the zero-point was calculated by Springob et al. (2014) to be 0.003 dex. We test the effect of this uncertainty on our bulk flow measurement, by repeating the analysis but first shifting all the η values by $+0.003$ dex or -0.003 dex. This changes the derived pecu-

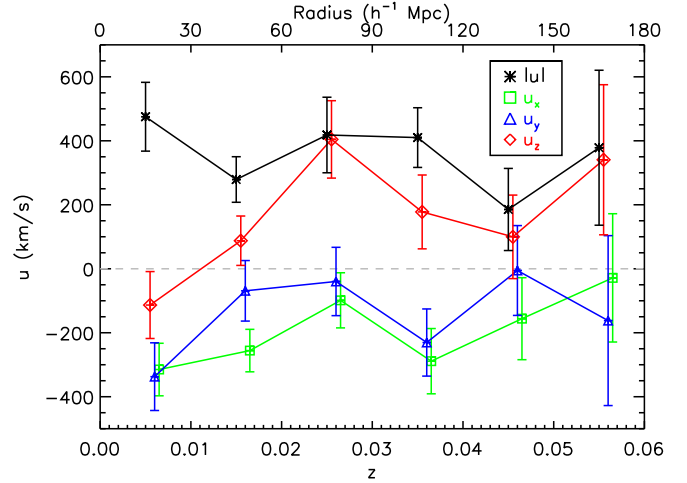


Figure 13. The MLE bulk flow for 6dFGSv in redshift shells of width $\Delta z = 0.01$. The coloured lines show the Equatorial (x, y, z) components (labelled) and are shifted to the right for clarity. The black line shows the bulk flow magnitude. The number of galaxies in each redshift shell is $\{75, 813, 1371, 2563, 2802, 1261\}$. The error bars indicate the noise uncertainty in each bin.

liar velocities v , the estimated velocity uncertainties σ_n (see Section 3), and the resulting bulk flow. We list the new σ_n and MV bulk flow values in Table 3.

The changes in the MV bulk flow values we find, after adding or subtracting 0.003 dex, are all smaller than the noise uncertainties on our bulk flow measurement. Hence the statistical uncertainty on the zero-point does not significantly affect our measurement.

There is also cosmic variance in the zero-point, i.e. in the net velocity of galaxies within the ‘great circle’, $-20^\circ \leq \text{Dec} \leq 0^\circ$. We can estimate this using our Λ CDM mock catalogues, as follows:

- (i) In each mock catalogue, calculate the mean radial component of peculiar velocity of galaxies within $-20^\circ \leq \text{Dec} \leq 0^\circ$.
- (ii) Then subtract this mean radial velocity from all of the galaxies in the mock.
- (iii) Calculate the MLE bulk flow of the mock before and after doing this.
- (iv) Calculate the vector difference between these.

Table 3. The effect of statistical uncertainty in the Fundamental Plane zero-point on the 6dFGS bulk flow measurements. The best-fit velocity uncertainty σ_n , and MV bulk flow magnitude $|\mathbf{U}|$ and Galactic latitude and longitude (l, b) , are listed for the 6dFGSv measurement after adding or subtracting the statistical uncertainty on the zero-point, 0.003 dex, from all the logarithmic distance ratios η .

Quantity measured	Amount by which we shift η values of all galaxies		
	−0.003 dex	0 dex (result)	+0.003 dex
σ_n	$0.326H_0D_z$	$0.324H_0D_z$	$0.322H_0D_z$
MV BF, $R_I = 50 h^{-1}$ Mpc			
$ \mathbf{U} $ (km s $^{-1}$)	$238 \pm 55(97)$	$248 \pm 58(100)$	$266 \pm 62(105)$
(l, b) (°)	$(324 \pm 25, 51 \pm 14)$	$(318 \pm 20, 40 \pm 13)$	$315 \pm 16, 30 \pm 12$
MV BF, $R_I = 70 h^{-1}$ Mpc			
$ \mathbf{U} $ (km s $^{-1}$)	$231 \pm 55(97)$	$243 \pm 58(101)$	$263 \pm 62(105)$
(l, b) (°)	$(324 \pm 26, 51 \pm 14)$	$(318 \pm 20, 39 \pm 13)$	$(314 \pm 16, 30 \pm 12)$

Table 4. Uncertainty in the 6dFGS MV and MLE bulk flow measurements due to cosmic variance in the Fundamental Plane zero-point. We list the RMS variance found from our mocks in Equatorial Cartesian coordinates (u_x, u_y, u_z) , Galactic coordinates (l, b) , Equatorial coordinates (RA, Dec) and bulk flow magnitude $|\mathbf{U}|$.

	δu_x (km s $^{-1}$)	δu_y (km s $^{-1}$)	δu_z (km s $^{-1}$)	δl (°)	δb (°)	δRA (°)	δDec (°)	$\delta \mathbf{U} $ (km s $^{-1}$)
MV BF, $R_I = 50 h^{-1}$ Mpc	3	8	128	28	21	2	25	51
MV BF, $R_I = 70 h^{-1}$ Mpc	3	8	128	30	22	2	25	52

We find the RMS variance in the mean radial peculiar velocity in the great circle, over all the mocks, is 82 km s^{-1} , and the RMS variance in logarithmic distance ratio η is 0.004 dex. The RMS variance in the vector shift in bulk flow, over all the mocks, is $(\delta u_x, \delta u_y, \delta u_z) = (3, 8, 128) \text{ km s}^{-1}$ in Equatorial cartesian coordinates, shown in Table 4. In other words, the zero-point calibration induces a RMS variance primarily in the north-south direction.

We note that if the net radial peculiar velocity in the ‘great circle’ is negative, i.e. towards the observer, then calibrating it to zero shifts the measured bulk flow to more negative Dec. If the net velocity is positive, then the shift is towards more positive Dec. Either way, there is negligible shift in RA, since 6dFGSv is fairly symmetrical in Equatorial x and y .

The cosmic variance this adds to our 6dFGSv bulk flow measurement depends on the direction and amplitude of the measurement. We show the resulting cosmic variance on the amplitude and direction of our MV bulk flow measurements at $R_I = 50$ and $70 h^{-1}$ Mpc in Table 4. The uncertainty on the bulk flow amplitude due to cosmic variance in the zero-point is $\sim 50 \text{ km s}^{-1}$, slightly smaller than the statistical uncertainty of 58 km s^{-1} .

6.7 Comparison with other results

We compare our bulk flow result to other recent measurements in the literature, in Table 5. Our result is one of the most precise to date, thanks to the large number of galaxies in 6dFGSv. Our MV result of $248 \pm 58 \text{ km s}^{-1}$ at $R_I = 50 h^{-1}$ Mpc is a significantly lower amplitude than that of WFH09 at the same scale, despite the fact that the 6dFGSv survey volume is smaller than the COMPOSITE sample that they use, and so might be expected to have more cosmic variance. The level of disagreement between our result and WFH09, not accounting for this volume difference, is 1.56σ . Our measurement also does not appear to support the high-redshift $600 - 1000 \text{ km s}^{-1}$ measurement of

Kashlinsky et al. (2008), although since their scale is much larger we cannot directly rule it out.

Our result is consistent with a growing number of recent measurements that find a bulk flow amplitude consistent with Λ CDM, including Colin et al. (2011), Dai et al. (2011), Nusser & Davis (2011), Turnbull et al. (2012), Feindt et al. (2013) and Carrick et al. (2014).

As we see in Table 5 and Figure 8, the direction of our bulk flow is much closer to Shapley than other bulk flow measurements. This is reasonable, since 6dFGSv covers only the southern hemisphere, and so the bulk flow we measure is likely to be dominated by large southern structures such as Shapley.

We note again that the different surveys quoted in this table all have different window functions, so even those at the same effective distance may not be directly comparable. In particular a region of a “quiet” Hubble flow has been identified in the northern sky (Courteau et al. 1993) which is in contrast to the southern sky that has large motions arising from the Great Attractor and the Shapley Supercluster (see e.g. Hudson et al. 1999; Feindt et al. 2013). If the Turnbull et al. (2012) SNIa dataset is sub-divided into north and south samples, the measured bulk flow amplitudes are 110 ± 90 and $320 \pm 120 \text{ km s}^{-1}$ respectively. As datasets improve such biases will need to be fully addressed.

As a final point, recently Johnson et al. (2014) measured the velocity power spectrum of the 6dFGSv dataset as a function of scale, and found it to be 1σ larger than the prediction given by a *Planck* cosmology on the largest scale they measured ($k = [0.005, 0.02]$). However, they find it to be consistent at the 2σ level. This is consistent with our fit to Ω_m and σ_8 in Figure 11, which is also consistent with *Planck* at the 1σ level. As Johnson et al. (2014) mention, this is not a significant disagreement with Λ CDM.

Table 5. Summary of some recent bulk flow results in the literature, compared to the result in this work. For each measurement, we list the distance indicator used (DI), the number of peculiar velocities in the sample N , the radius of the measurement R , the measured bulk flow magnitude $|\mathbf{U}|$, and the direction of the bulk flow in Galactic longitude l and latitude b . A dash for the DI means a combination of datasets were used – these results all used the COMPOSITE sample. For measurements of the kSZ effect, N shows the number of clusters used in combination with the CMB (with the exception of Lavaux (2013), who use galaxies instead of clusters). A number of these results use the same, or overlapping, datasets, but apply different analyses, and the window functions differ for each survey.

	DI	N	R (h^{-1} Mpc)	$ \mathbf{U} $ (km s^{-1})	l ($^{\circ}$)	b ($^{\circ}$)
6dFGSv (this work)	FP	8885	50	248 ± 58	318 ± 20	40 ± 13
	FP	8885	70	243 ± 58	318 ± 20	39 ± 13
Dressler et al. (1987a)	FP	423	$\lesssim 60$	599 ± 104	312 ± 11	6 ± 10
Watkins et al. (2009)	Mix	4481	50	407 ± 81	287 ± 9	8 ± 6
Feldman et al. (2010)	Mix	4536	50	416 ± 78	282 ± 11	6 ± 6
Macaulay et al. (2012)	Mix	4537	33	380^{+99}_{-132}	295 ± 18	14 ± 18
Ma & Scott (2013)	Mix	3304	50	340 ± 40	280 ± 8	5.1 ± 6
Nusser & Davis (2011)	TF	2859	40	333 ± 38	276 ± 3	14 ± 3
Ma & Pan (2014)	TF	2915	58	290 ± 30	281 ± 7	8^{+6}_{-5}
Colin et al. (2011)	SNe	142	160	260 ± 150	298^{+62}_{-48}	8^{+34}_{-52}
Dai et al. (2011)	SNe	132	150	188^{+199}_{-103}	290^{+39}_{-31}	20 ± 32
Turnbull et al. (2012)	SNe	254	50	249 ± 76	319 ± 18	7 ± 14
Feindt et al. (2013) ^a	SNe	128	74	243 ± 88	298 ± 25	15 ± 20
Weyant et al. (2011)	SNe	30	112	446 ± 101	273 ± 11	46 ± 8
Kashlinsky et al. (2008)	kSZ	782	$\sim 300 - 800$	$\sim 600 - 1000$	283 ± 14	12 ± 14
Planck Collaboration (2013)	kSZ	1405	350	< 390 (95% CL)	~ 120	~ 34
			2000	< 254 (95% CL)		
Lavaux (2013)	kSZ	5290	50	533 ± 263	324 ± 27	-7 ± 17
			200	284 ± 187	26 ± 35	-17 ± 19
			~ 500	< 470 (95% CL)		

^a The result for their lowest redshift shell

6.8 Implications for Cosmography

An important aim for bulk flow measurements has been to understand the motion of the Local Group (LG) with respect to the CMB, of $627 \pm 22 \text{ km s}^{-1}$ towards $l = 276 \pm 3^{\circ}$, $b = 30 \pm 2^{\circ}$ (Kogut et al. 1993). From gravitational instability theory, this is expected to be caused by nearby structures, and to converge to the CMB dipole beyond them.

As we showed in Figure 8, the direction of our bulk flow is consistent with the direction of the Shapley Supercluster. We also saw in Figure 13 that the amplitude of the bulk flow remains fairly constant with distance, indicating that it is sourced by a distant rather than a nearby overdensity. This therefore seems to indicate that Shapley may be the dominant source of the bulk flow motion we detect. Shapley is at a distance of $152 h^{-1} \text{ Mpc}$, and is the largest supercluster in the local Universe out to $200 h^{-1} \text{ Mpc}$ (Lavaux & Hudson 2011). Our result is consistent with many other bulk flow measurements that find directions close to Shapley (e.g. Feindt et al. 2013) and a source distance greater than $\sim 50 - 80 h^{-1} \text{ Mpc}$ as the origin of the flow (e.g. Hudson 1994; Kocevski et al. 2004; Pike & Hudson 2005; Watkins et al. 2009).

Lavaux & Hudson (2011) calculate, using linear theory applied to 6dFGS redshift data, that Shapley should be responsible for ~ 15 per cent of the total velocity of the LG with respect to the CMB, or $90 \pm 10 \text{ km s}^{-1}$, while the Horologium-Reticulum supercluster generates $\sim 60 \text{ km s}^{-1}$. However, it appears that our sample is dominated mostly by Shapley. This makes it possible that its mass could be even larger than inferred from redshift data alone, which

would agree with the finding of Feindt et al. (2013), who find that the bulk flow does not appear to reverse beyond Shapley, suggesting there could be more mass beyond it sourcing the bulk flow. They calculate that their bulk flow would be caused either if the mass of Shapley were twice as large as current estimates (from Muñoz & Loeb 2008; Sheth & Diaferio 2011), or if there were a more distant mass behind Shapley.

As we have previously noted however, 6dFGSv partially samples the Shapley region, with no sampling at all of northern-sky structures, so this could be partially responsible for Shapley dominating our results. Additionally, Springob et al. (2014) show that the 6dFGSv sample shows not only an excess of positive velocities towards Shapley, but also an excess of negative velocities on the other side of the sky towards the Cetus Supercluster, compared to model predictions, indicating other structures are also contributing to the velocity dipole of the sample. As we found in Section 6.6, the cosmic variance in the zeropoint of the Fundamental Plane also gives additional angular uncertainty to our measurement in the north-south direction. More analysis would therefore be needed to confirm whether the bulk flow is truly closer to Shapley than any other structure.

7 CONCLUSION

The question of whether a large bulk flow exists in the local Universe remains of much interest. A large part of the disagreement between previous measurements is likely due to the noisy, sparse peculiar velocity samples to date, as well as

possible unknown systematics such as differently-calibrated datasets and Malmquist (or selection) biases. In this paper we aimed to make an improved measurement using a large new peculiar velocity dataset, the 6 degree Field Galaxy Survey peculiar velocity sample (6dFGSv). This sample is homogeneously selected, so avoids any bias from combining datasets, and the uncertainties and Malmquist biases have been carefully studied and accounted for (M12, S14).

We have presented a new bulk flow analysis using this dataset. Using the ‘Minimum Variance’ bulk flow estimator, we find a bulk flow of magnitude $|\mathbf{U}| = 248 \pm 58 \text{ km s}^{-1}$ in the direction $(l, b) = (318^\circ \pm 20^\circ, 40^\circ \pm 13^\circ)$ at a distance of $50 h^{-1} \text{ Mpc}$, and $|\mathbf{U}| = 243 \pm 58 \text{ km s}^{-1}$ in the direction $(l, b) = (318^\circ \pm 20^\circ, 39^\circ \pm 13^\circ)$ at a distance of $70 h^{-1} \text{ Mpc}$. This is somewhat higher than the ΛCDM prediction on these scales, implying a high value of σ_8 , but consistent with *Planck* results within 2σ . After marginalising over Ω_m , we find from our bulk flow measurement at $R_I = 70 h^{-1} \text{ Mpc}$ a value of $\sigma_8 = 1.01^{+1.07}_{-0.58}$, consistent with the *Planck* value of 0.83 within 68.27% confidence.

Our result is in agreement with a number of recent measurements that also find a bulk flow consistent with ΛCDM , including Turnbull et al. (2012), Feindt et al. (2013) and Hong et al. (2014). Our result is also supported by the higher-redshift measurement of Planck Collaboration et al. (2014b), who used *Planck* CMB data combined with a large X-ray cluster catalogue, and found no evidence for a bulk flow from $350 h^{-1} \text{ Mpc}$ to $2 h^{-1} \text{ Gpc}$ scales.

A challenge for the 6dFGSv analysis here (and for any peculiar velocity analysis made using linear velocities instead of log distances) is accounting for the lognormal uncertainties on the peculiar velocities. When combined with the fact that 6dFGSv only covers half the sky, these can result in a spurious polar bulk flow component if not properly accounted for. We have shown that it is important to propagate uncertainty from the Gaussian observable (in our case, the logarithmic distance ratio $\eta = \log_{10} D_z/D_r$) to the non-Gaussian velocity in a way that is independent of the $\eta \rightarrow v$ conversion itself, so that the velocity uncertainties, and hence bulk flow weights, do not correlate with the velocities. A further effect may come from the fact that the distribution of measured velocities themselves will be affected by the lognormal uncertainties. A possible solution to this problem was recently suggested by Watkins & Feldman (2015). We leave investigation of this for 6dFGSv to future work.

Our measured bulk flow is very close to the direction of the Shapley Supercluster, consistent with many other measurements, and its amplitude appears to be fairly constant out to the distance of Shapley. This suggests that a large part of the bulk flow we measure is likely to be sourced by Shapley, which is reasonable since 6dFGSv is a southern-sky survey.

Finally, we have also generated a set of ΛCDM mock catalogues of 6dFGSv, based on the GigggleZ N -body simulation and incorporating the 6dFGSv selection function, to be used for testing systematic biases in the dataset. We find the 6dFGSv bulk flow amplitude is consistent with the distribution measured in the mocks. Using the mocks, we also estimate the additional uncertainty in our bulk flow amplitude, due to cosmic variance in the Fundamental Plane zero-point, to be $\sim 50 \text{ km s}^{-1}$.

These mocks are available on request for fur-

ther analyses of the 6dFGSv sample. The C++ code written to calculate the Minimum Variance bulk flow for this paper is publicly available on GitHub, at <https://github.com/mscrim/MVBulkFlow>.

8 ACKNOWLEDGEMENTS

We thank Hume Feldman and Richard Watkins for assistance with the MV implementation, and we also thank Hume and Pirin Erdoğdu for helpful comments on this draft. Thanks also to Matt George and Jon Carrick for helpful discussions.

M.I.S. acknowledges financial support from a Jean Rogerson Scholarship, a UWA Top-up Scholarship from the University of Western Australia, and a CSIRO Malcolm McIntosh Lecture bankmecu scholarship. M.I.S. thanks the Astronomical Society of Australia for providing financial support via a Student Travel Award, which enabled further collaboration on this paper, and also Lawrence Berkeley National Laboratory for hosting her during part of this work. CB and TMD acknowledge the support of the Australian Research Council through the award of Future Fellowships, grants FT110100639 and FT100100595 respectively. The Centre for All-sky Astrophysics is an Australian Research Council Centre of Excellence, funded by grant CE110001020.

REFERENCES

- Aaronsen, M., Bothun, G., Mould, J., Huchra, J., Schommer, R. A., & Cornell, M. E. 1986, *ApJ*, 302, 536
- Abate, A., & Feldman, H. A. 2012, *MNRAS*, 419, 3482, 1106.5791
- Agarwal, S., Feldman, H. A., & Watkins, R. 2012, *MNRAS*, 424, 2667, 1201.0128
- Bahcall, N. A., Gramann, M., & Cen, R. 1994, *ApJ*, 436, 23, astro-ph/9410061
- Bertschinger, E., Dekel, A., Faber, S. M., Dressler, A., & Burstein, D. 1990, *ApJ*, 364, 370
- Bilicki, M., Chodorowski, M., Jarrett, T., & Mamon, G. A. 2011, *ApJ*, 741, 31, 1102.4356
- Campbell, L. A. 2009, PhD thesis, The Australian National University
- Campbell, L. A. et al. 2014, *MNRAS*, 443, 1231, 1406.4867
- Carrick, J., Turnbull, S. J., Lavaux, G., & Hudson, M. 2014, submitted
- Coles, P., & Lucchin, F. 2002, *Cosmology: The Origin and Evolution of Cosmic Structure*, Second Edition
- Colin, J., Mohayaee, R., Sarkar, S., & Shafieloo, A. 2011, *MNRAS*, 414, 264, 1011.6292
- Courteau, S., Faber, S. M., Dressler, A., & Willick, J. A. 1993, *ApJL*, 412, L51
- Dai, D.-C., Kinney, W. H., & Stojkovic, D. 2011, *JCAP*, 4, 15, 1102.0800
- Davis, T. M., & Lineweaver, C. H. 2004, *PASA*, 21, 97, arXiv:astro-ph/0310808
- Davis, T. M., & Scrimgeour, M. I. 2014, *MNRAS*, 442, 1117, 1405.0105
- de Vaucouleurs, G., & Peters, W. L. 1984, *ApJ*, 287, 1

- Dekel, A., Eldar, A., Kolatt, T., Yahil, A., Willick, J. A., Faber, S. M., Courteau, S., & Burstein, D. 1999, *ApJ*, 522, 1, arXiv:astro-ph/9812197
- Dressler, A., Faber, S. M., Burstein, D., Davies, R. L., Lynden-Bell, D., Terlevich, R. J., & Wegner, G. 1987a, *ApJL*, 313, L37
- Dressler, A., Lynden-Bell, D., Burstein, D., Davies, R. L., Faber, S. M., Terlevich, R., & Wegner, G. 1987b, *ApJ*, 313, 42
- Erdoğan, P. et al. 2006a, *MNRAS*, 368, 1515, astro-ph/0507166
- . 2006b, *MNRAS*, 373, 45, arXiv:astro-ph/0610005
- Feindt, U. et al. 2013, *A & A*, 560, A90, 1310.4184
- Feix, M., Nusser, A., & Branchini, E. 2014, *JCAP*, 9, 19, 1405.6710
- Feldman, H. A., Watkins, R., & Hudson, M. J. 2010, *MNRAS*, 407, 2328, 0911.5516
- Guzzo, L. et al. 2008, *Nat*, 451, 541, 0802.1944
- Harrison, E. 1993, *ApJ*, 403, 28
- Hart, L., & Davies, R. D. 1982, *Nat*, 297, 191
- Hogg, D. W. 1999, *ArXiv Astrophysics e-prints*, arXiv:astro-ph/9905116
- Hogg, D. W., Eisenstein, D. J., Blanton, M. R., Bahcall, N. A., Brinkmann, J., Gunn, J. E., & Schneider, D. P. 2005, *ApJ*, 624, 54, arXiv:astro-ph/0411197
- Hong, T. et al. 2014, submitted
- Hudson, M. J. 1994, *MNRAS*, 266, 475
- Hudson, M. J., Smith, R. J., Lucey, J. R., Schlegel, D. J., & Davies, R. L. 1999, *ApJL*, 512, L79, astro-ph/9901001
- Jarrett, T.-H., Chester, T., Cutri, R., Schneider, S., Rosenberg, J., Huchra, J. P., & Mader, J. 2000, *AJ*, 120, 298, arXiv:astro-ph/0005017
- Johnson, A. et al. 2014, *ArXiv e-prints*, 1404.3799
- Jones, B. J., Martínez, V. J., Saar, E., & Trimble, V. 2004, *Reviews of Modern Physics*, 76, 1211, arXiv:astro-ph/0406086
- Jones, D. H., Peterson, B. A., Colless, M., & Saunders, W. 2006, *MNRAS*, 369, 25, arXiv:astro-ph/0603609
- Jones, D. H. et al. 2009, *MNRAS*, 399, 683, 0903.5451
- Kaiser, N. 1987, *MNRAS*, 227, 1
- . 1988, *MNRAS*, 231, 149
- Kashlinsky, A., Atrio-Barandela, F., Kocevski, D., & Ebeling, H. 2008, *ApJL*, 686, L49, 0809.3734
- Keisler, R. 2009, *ApJL*, 707, L42, 0910.4233
- Kocevski, D. D., & Ebeling, H. 2006, *ApJ*, 645, 1043, astro-ph/0510106
- Kocevski, D. D., Mullis, C. R., & Ebeling, H. 2004, *ApJ*, 608, 721, astro-ph/0403275
- Kogut, A. et al. 1993, *ApJ*, 419, 1, astro-ph/9312056
- Lavaux, G., Afshordi, N., & Hudson, M. J. 2013, *MNRAS*, 430, 1617, 1207.1721
- Lavaux, G., & Hudson, M. J. 2011, *MNRAS*, 416, 2840, 1105.6107
- Lavaux, G., Tully, R. B., Mohayaee, R., & Colombi, S. 2010, *ApJ*, 709, 483, 0810.3658
- Lewis, A., Challinor, A., & Lasenby, A. 2000, *ApJ*, 538, 473, arXiv:astro-ph/9911177
- Li, M. et al. 2012, *ApJ*, 761, 151, 1207.5338
- Lynden-Bell, D., Faber, S. M., Burstein, D., Davies, R. L., Dressler, A., Terlevich, R. J., & Wegner, G. 1988, *ApJ*, 326, 19
- Ma, Y.-Z., Gordon, C., & Feldman, H. A. 2011, *Phys. Rev. D*, 83, 103002, 1010.4276
- Ma, Y.-Z., & Pan, J. 2014, *MNRAS*, 437, 1996, 1311.6888
- Ma, Y.-Z., & Scott, D. 2013, *MNRAS*, 428, 2017, 1208.2028
- Macaulay, E., Feldman, H. A., Ferreira, P. G., Jaffe, A. H., Agarwal, S., Hudson, M. J., & Watkins, R. 2012, *MNRAS*, 425, 1709, 1111.3338
- Magoulas, C. et al. 2012, *MNRAS*, 427, 245, 1206.0385 (M12)
- . 2015, in preparation
- Muñoz, J. A., & Loeb, A. 2008, *MNRAS*, 391, 1341, 0805.0596
- Nusser, A., & Davis, M. 2011, *ApJ*, 736, 93, 1101.1650
- Nusser, A., Davis, M., & Branchini, E. 2014, *ApJ*, 788, 157, 1402.6566
- Osborne, S. J., Mak, D. S. Y., Church, S. E., & Pierpaoli, E. 2011, *ApJ*, 737, 98, 1011.2781
- Peacock, J. A. et al. 2001, *Nat*, 410, 169, arXiv:astro-ph/0103143
- Peebles, P. J. E. 1980, *The large-scale structure of the universe*
- Pike, R. W., & Hudson, M. J. 2005, *ApJ*, 635, 11, astro-ph/0511012
- Planck Collaboration et al. 2014a, *A & A*, 571, A16, 1303.5076
- . 2014b, *A & A*, 561, A97, 1303.5090
- Poole, G. B. et al. 2014, *ArXiv e-prints*, 1407.0390
- Rubin, V. C., Thonnard, N., Ford, Jr., W. K., & Roberts, M. S. 1976, *AJ*, 81, 719
- Scrimgeour, M. I. et al. 2012, *MNRAS*, 425, 116, 1205.6812
- Sheth, R. K., & Diaferio, A. 2011, *MNRAS*, 417, 2938, 1105.3378
- Smith, R. E. et al. 2003, *MNRAS*, 341, 1311, arXiv:astro-ph/0207664
- Springel, V., Yoshida, N., & White, S. D. M. 2001, *NewA*, 6, 79, arXiv:astro-ph/0003162
- Springob, C. M. et al. 2014, *MNRAS*, 445, 2677, 1409.6161
- Strauss, M. A., & Willick, J. A. 1995, *Phys. Rep.*, 261, 271, arXiv:astro-ph/9502079
- Tegmark, M. et al. 2004, *ApJ*, 606, 702, arXiv:astro-ph/0310725
- Turnbull, S. J., Hudson, M. J., Feldman, H. A., Hicken, M., Kirshner, R. P., & Watkins, R. 2012, *MNRAS*, 420, 447, 1111.0631
- Watkins, R., & Feldman, H. A. 2015, *MNRAS*, 450, 1868, 1411.6665
- Watkins, R., Feldman, H. A., & Hudson, M. J. 2009, *MNRAS*, 392, 743, 0809.4041 (WFH09)
- Weyant, A., Wood-Vasey, M., Wasserman, L., & Freeman, P. 2011, *ApJ*, 732, 65, 1103.1603
- Willick, J. A., & Strauss, M. A. 1998, *ApJ*, 507, 64, arXiv:astro-ph/9801307

APPENDIX A: MINIMUM VARIANCE BULK FLOW METHOD FROM WATKINS ET AL. (2009)

For a dataset consisting of N peculiar velocities with positions $\mathbf{r}_n = x_i$, where i indicates the 3 directions (x, y, z), and measured radial peculiar velocities S_n , the MV method (Watkins et al. 2009; Feldman et al. 2010) constructs a set

of weights $w_{i,n}$ such that the bulk flow is given by equation 12. The weights act to minimise the variance between the bulk flow moments measured by the survey, u_i , and the bulk flow moments that would be measured by an ‘ideal’ survey, U_i .

To calculate the weights, the authors apply constraints to ensure that the estimator gives the correct average amplitudes for the velocity moments, i.e. $\langle u_i \rangle = U_i$, of the form

$$\sum_n w_{i,n} g_j(\mathbf{r}_n) = \delta_{ij}. \quad (\text{A1})$$

Here, $g_j(\mathbf{r})$ are the mode functions corresponding to given moments of the velocity field; for the three bulk flow moments, they are

$$g_j(\mathbf{r}) = \{\hat{\mathbf{r}}_x, \hat{\mathbf{r}}_y, \hat{\mathbf{r}}_z\}. \quad (\text{A2})$$

The authors implement the set of constraints in Equation A1 using Lagrange multipliers, and so the quantity to be minimised is

$$\langle (U_i - u_i)^2 \rangle + \sum_j \lambda_{ij} \left[\sum_n w_{i,n} g_j(\mathbf{r}_n) - \delta_{ij} \right]. \quad (\text{A3})$$

Feldman et al. (2010) show that the weights can be evaluated as:

$$w_{i,n} = \sum_m G_{nm}^{-1} \left(Q_{im} - \frac{1}{2} \sum_j \lambda_{ij} g_j(\mathbf{r}_m) \right). \quad (\text{A4})$$

We define the matrices G , Q and λ below.

A1 Velocity covariance matrix, G

$G_{nm} = \langle S_n S_m \rangle$ is the covariance matrix for the individual velocities, which can be calculated for a given power spectrum. In linear theory it can be written in terms of the velocity field $\mathbf{v}(\mathbf{r})$ as

$$\begin{aligned} G_{nm} &= \langle S_n S_m \rangle \\ &= \langle v_n v_m \rangle + \delta_{nm} (\sigma_*^2 + \sigma_n^2). \end{aligned} \quad (\text{A5})$$

The first, ‘geometrical’ term can be expressed as an integral over the density power spectrum $P(k)$:

$$\langle v_n v_m \rangle = \frac{f(\Omega_m, z)^2 H_0^2 a^2}{2\pi^2} \int dk P(k) f_{mn}(k), \quad (\text{A6})$$

where H_0 is the Hubble constant in units of ($h \text{ km s}^{-1} \text{ Mpc}^{-1}$), a is the cosmological scale factor, essentially equal to unity for the low redshifts we are considering, and the function $f_{mn}(k)$ is the angle averaged window function,

$$f_{mn}(k) = \int \frac{d^2 \hat{\mathbf{k}}}{4\pi} (\hat{\mathbf{r}}_n \cdot \hat{\mathbf{k}})(\hat{\mathbf{r}}_m \cdot \hat{\mathbf{k}}) \exp[ik \hat{\mathbf{k}} \cdot (\mathbf{r}_n - \mathbf{r}_m)]. \quad (\text{A7})$$

This equation can be calculated analytically, as shown in the appendix of Ma et al. (2011).

A2 Velocity-bulk flow cross correlation, Q

The correlation matrix $Q_{i,n}$ is calculated in a similar way, but incorporates the window function of the input ‘ideal’ survey. It is evaluated by generating an ideal survey with

N' random positions $\mathbf{r}'_{n'}$ with the desired radial distribution function. $Q_{i,n}$ is then given by

$$Q_{i,n} = \langle U_i v_n \rangle = \sum_{n'=1}^{N'} w'_{i,n'} \langle v_{n'} v_n \rangle. \quad (\text{A8})$$

The weights $w'_{i,n'}$ for the ideal survey simply give the bulk flow as the average of the projections of the radial velocities on the three coordinate axis directions,

$$w_{i,n} = \frac{3\hat{\mathbf{x}}_i \cdot \hat{\mathbf{r}}_n}{N}. \quad (\text{A9})$$

(Note in WFH09 the factor of 3 has been omitted from this equation). Following Watkins et al. (2009) we create an ‘ideal’ survey with $N' = 10^4$ and a Gaussian radial density $n(r) \propto \exp(-r^2/2R_I^2)$, where R_I is the effective radius of the Gaussian.

Then, we evaluate $\langle v_{n'} v_n \rangle$ by

$$\langle v_{n'} v_n \rangle = \frac{f(\Omega_m, z)^2 H_0^2 a^2}{2\pi^2} \int dk P(k) f_{n'n}(k). \quad (\text{A10})$$

A3 Lagrange multiplier, λ

The Lagrange multiplier λ_{ij} is given by

$$\lambda_{ij} = \sum_{l=1}^3 \left[M_{il}^{-1} \left(\sum_{m,n} G_{nm}^{-1} Q_{lm} g_j(\mathbf{r}_n) - \delta_{lj} \right) \right] \quad (\text{A11})$$

where

$$M_{ij} = \frac{1}{2} \sum_{n,m} G_{nm}^{-1} g_i(\mathbf{r}_n) g_j(\mathbf{r}_m). \quad (\text{A12})$$

For the bulk flow, with $g_i(\mathbf{r}) = \hat{\mathbf{r}}_i$, the latter equation becomes

$$M_{ij} = \frac{1}{2} \sum_{n,m} G_{nm}^{-1} \hat{\mathbf{r}}_i(n) \hat{\mathbf{r}}_j(m). \quad (\text{A13})$$